Human papillomavirus E7 inhibits immune responses in keratinocytes by activating HTRA1-mediated mitophagy

BOYA ZHANG[1], DEFENG KONG[1], SIJI CHEN[1], XUEWU SUN[2] and HAO CHENG[1]

[1]Department of Dermatology, Sir Run Run Shaw Hospital, School of Medicine, Zhejiang University, Hangzhou, Zhejiang 310016, P.R. China; [2]Department of Orthopedic Surgery, Sir Run Run Shaw Hospital, School of Medicine, Zhejiang University, Hangzhou, Zhejiang 310016, P.R. China

Received July 4, 2025; Accepted October 22, 2025

DOI: 10.3892/ijmm.2025.5693

Abstract. Persistent infection with human papillomavirus (HPV) can lead to refractory disease. The HPV E7 protein causes persistent viral infection by disrupting the immune balance of keratinocytes; however, its key mechanism is not yet clear. Overexpression of the HPV E7 gene in normal human epidermal keratinocytes can promote mitophagy in the host cells and inhibit the expression of type I interferon (IFN), as previously confirmed by electron microscopy, immunofluorescence and western blot analysis. In the present study, Siha cells with stable knockdown of HPV16 E7 were constructed, and RNA sequencing at the transcription level and isobaric tags for relative and absolute quantitation analysis at the protein level were performed, with the aim of identifying genes related to mitophagy among the differentially expressed genes. Using immunohistochemistry, PCR and western blotting, significant differences were detected in the expression levels of high-temperature requirement A serine peptidase 1 (HTRA1) between the knockdown and control groups. The results confirmed that HPV E7 could promote the expression of HTRA1. Furthermore, it was demonstrated that the HPV E7 protein interacted with HTRA1 intracellularly to activate the PTEN-induced kinase 1 (PINK1)/Parkin pathway in keratinocytes, leading to enhanced mitophagy and reduced expression of type I IFN in host cells. In conclusion, HPV E7 could promote the expression of the HTRA1 gene in keratinocytes, thereby activating mitophagy mediated by the PINK1/Parkin pathway. Furthermore, HPV E7 could inhibit the secretion of type I IFN from cells, thus leading to persistent viral infection. These findings provide novel insights into the association between HPV infection and mitophagy, and may elucidate the mechanisms underlying persistent HPV infection.

Correspondence to: Dr Hao Cheng, Department of Dermatology, Sir Run Run Shaw Hospital, School of Medicine, Zhejiang University, 3 Qingchun East Road, Hangzhou, Zhejiang 310016, P.R. China
E-mail: chenghao1@zju.edu.cn

Dr Xuewu Sun, Department of Orthopedic Surgery, Sir Run Run Shaw Hospital, School of Medicine, Zhejiang University, 3 Qingchun East Road, Hangzhou, Zhejiang 310016, P.R. China
E-mail: xuewu_sun@zju.edu.cn

Key words: human papillomavirus, E7 protein, mitophagy, PTEN-induced kinase 1/Parkin, type I interferon, immune response

Introduction

Human papillomavirus (HPV) is a small double-stranded DNA virus, for which >200 genotypes have thus far been identified (1). HPV infection can alter the host cellular immune response, including suppression of interferon (IFN) production, which impairs viral clearance and leads to persistent infection, thereby contributing to the development of various associated diseases (2,3). Currently, HPV is classified into low- and high-risk types based on the degree of pathogenicity. High-risk HPV is closely associated with various malignancies, including cervical and anal cancer, whereas low-risk HPV infections are mainly associated with verrucous hyperplasia of the skin and mucous membranes, such as condyloma acuminatum (4,5). The HPV genome contains eight open reading frames and is organized into three functional regions: The early region, the late region and the long control region. The early region encodes six non-structural proteins: E1, E2, E4, E5, E6 and E7 (6); among these, E1, E2, E4 and E5 are involved in viral DNA replication, whereas E6 and E7 are recognized as the primary oncoproteins responsible for cellular transformation (7). The E7 protein is an acidic polypeptide consisting of 98-105 amino acids (aa) (8). E7 exhibits multiple biological functions and has been shown to interact with key regulatory proteins, including pRB, p107, p130, MPP2 and DNA methyltransferase 1, thereby modulating their activities. These interactions contribute to the dysregulation of critical cellular processes, such as cell proliferation, differentiation, migration, survival and apoptosis (9-12). With the growing progression of attitudes towards sexual relationships, the infection rate of HPV is increasing annually (13-15). In recent years, a large-scale multicenter study in China has demonstrated that the overall prevalence of HPV among women is 17.70%, representing an upward trend compared with the prevalence rate reported in the same population group in 2008 (16.1%) (16). Furthermore, the age of onset of HPV-related diseases is decreasing and the locations of onset are variable,

thus making HPV more difficult to treatment (17). Notably, the current therapeutic options for HPV-related diseases remain relatively limited (18). For example, for cervical cancer resulting from high-risk HPV, surgical removal of the lesion is frequently performed in clinical practice (19,20). By contrast, condyloma acuminatum caused by low-risk HPV can be alleviated by physical methods, such as microwave treatment and cryotherapy for wart removal (21,22). However, as there has been no breakthrough yet in research on the specific mechanism underlying persistent HPV infection, effective means to completely eliminate HPV are still lacking in the clinical setting. Therefore, a radical cure has not yet been achieved in clinical practice Recurrent disease not only exerts a profound impact on the physical and mental health of patients, but also imposes considerable economic burdens on their families and society at large. Thus, studying the mechanism underlying persistent HPV infection is a current focus of research. Subsequently, exploring drugs and methods for specific viral clearance after HPV infection may be of important medical relevance and social value, with the aim of preventing and treating diseases associated with HPV infection.

The immune system, functioning as a pivotal system responsible for immune responses and functions, encompasses diverse cell types, tissues and organs that operate together to shield the entire organism from the invasion of various pathogens (23,24). Notably, the role of energy metabolism in immune regulation has garnered increasing attention in previous years (25,26). Mitophagy, constituting a specific type of autophagy that selectively eliminates dysfunctional mitochondria, has garnered increasing attention regarding its association with the immune functions of the body (27). Mitophagy can influence the immune functions of host cells through multiple modalities, including inhibiting the activation of inflammasomes, interfering with the expression of type I IFNs and suppressing the initiation of apoptosis in host cells (28,29).

Previous studies have demonstrated that mitophagy can impact the innate immune state of cells by suppressing activation of the NLRP3 inflammasome, and can serve a crucial role in cellular immune responses by regulating proteins, including mitochondrial antiviral signaling protein, retinoic acid-inducible gene I, melanoma differentiation-associated protein 5 and stimulator of IFN genes (STING), to inhibit the expression of type I IFNs (30-34). Knocking out the expression of mitophagy-related genes can release a considerable quantity of cytochrome *c* into the cytoplasm, thereby impeding the activation of caspase-3/-7 and suppressing apoptosis (35). Thus, mitophagy is closely associated with the immune functions of cells. According to the variance in autophagosome recognition pathways, mitophagy is classified into two types: i) Ubiquitin-related mitophagy, mediated by the PTEN-induced kinase 1 (PINK1)/Parkin (a RING-between-RING E3 ubiquitin protein ligase) pathway (36,37); and ii) ubiquitin-independent mitophagy, mediated by the Bcl-2 and adenovirus E1B 19 kDa-interacting protein 3 (BNIP3)/BNIP3-like (BNIP3L) pathway (38).

Currently, a considerable number of studies (28,39,40) have focused on the impact of viruses on the mitophagy of host cells. Viruses such as hepatitis B virus (HBV), hepatitis C virus (HCV), herpes simplex virus (HSV) and human immunodeficiency virus (HIV) can induce the mitophagy of host cells to suppress innate immunity and maintain a persistent infection. Notably, viruses can directly recognize mitophagy pathway proteins to influence mitophagy in host cells or can indirectly affect the level of mitophagy by influencing the metabolic status of host cells. For example, HBV can promote mitophagy by activating the PINK1/Parkin pathway, thereby facilitating viral replication (41). The viral IFN regulatory factor 1 encoded by human herpesvirus type 8 can directly bind to BNIP3L, activating mitophagy to enhance its replication within the host (42). Simultaneously, the non-structural protein 5A of HCV can activate mitophagy by increasing the generation of reactive oxygen species (ROS) (43). In the early stage after HIV infection, the single-stranded RNA of HIV type 1 activates mitophagy by increasing the generation of ROS and causing mitochondrial membrane depolarization (44). Emerging evidence has indicated that HPV is implicated in the regulation of mitophagy (45,46). These aforementioned research findings suggest that viruses can affect the immune response of host cells by influencing the intracellular level of mitophagy, thereby perpetuating the infection of host cells.

The present study aimed to investigate the impact of the early protein E7 of HPV on mitophagy pathway activity and to further assess the mechanism underlying persistent HPV infection.

Materials and methods

Cell culture. Primary normal human epidermal keratinocytes (NHEKs) were purchased from ScienCell Research Laboratories, Inc. and were cultured in Epilife medium, without any antibiotics, supplemented with 10% fetal bovine serum (FBS) and Human Keratinocyte Growth Supplement (all from Gibco; Thermo Fisher Scientific, Inc.) according to the manufacturer's instructions. Siha and 293T cells (The Cell Bank of Type Culture Collection of The Chinese Academy of Sciences) were cultured in DMEM (Gibco; Thermo Fisher Scientific, Inc.) supplemented with 10% FBS, 100 U/ml penicillin and 100 μg/ml streptomycin. All cells were cultured at 37˚C in the presence of 5% CO_2.

Construction of HPV11/16 E7-expressing and HTRA1-expressing NHEKs. The HPV11 E7 gene was amplified from the pBR322 vector [cat. no. 45151D; American Type Culture Collection (ATCC)] and HPV16 E7 gene was amplified from the pBluescript SK-vector (cat. no. 45113; ATCC). These two vectors contain the full-length genomes of HPV11 and HPV16, respectively. The amplified E7 genes were then cloned into the pcDNA3.1 vector (cat. no. V79020; Invitrogen; Thermo Fisher Scientific, Inc.). Subsequently, HPV11/16 E7 were cloned from the pcDNA3.1 vector into the pHAGE-fEF1a-IRES-ZsGreen lentiviral expression vector (provided by Professor Xiaojian Wang, Institute of Immunology, Zhejiang University, Hangzhou, China). In addition, the gene encoding Flag-HTRA1 was synthesized via full-gene synthesis and subsequently cloned into pHAGE-fEF1a-IRES-ZsGreen lentiviral expression vector. The empty pHAGE-fEF1a-IRES-ZsGreen lentiviral expression vector was used as a negative control. Lentiviral packaging used the 2nd generation system. For transfection,

293T cells cultured to 90% confluence were used; lentiviral, packaging (psPAX2; provided by Professor Xiaojian Wang) and envelope (pMD2.G; provided by Professor Xiaojian Wang) plasmids were co-transfected at a 4:3:1 molar ratio (total DNA: 12 μg) using PolyJet™ *In Vitro* DNA Transfection Reagent (cat. no. SL100688; SignaGen Laboratories) at 37˚C for 8 h, and viral supernatants were collected at 72 h post-transfection. NHEKs were then infected with lentiviruses at a multiplicity of infection (MOI) of 20, with medium replaced 24 h post-infection. Stable cell lines were selected using puromycin; 72 h post-infection, fluorescent protein expression was assessed under a fluorescence microscope (IX83; Olympus Corporation), and when fluorescent cells reached ~30%, they were cultured for another 48 h before selection with 2 μg/ml puromycin. The medium was changed every 24 h during selection, and the same puromycin concentration was maintained for subsequent cultures. Stable cell pools were ready for downstream experiments 1 week after selection initiation. Western blotting verified the successful expression of HPV11/16 E7 and HTRA1 in NHEKs.

Knockdown of HPV16 E7 and HTRA1. The HPV16 E7 short hairpin (sh)RNA sequence was cloned into the hU6-MCS-Ubiquitin-EGFP-IRES-puromycin vector (cat. no. GV248; Shanghai GeneChem Co., Ltd.). shRNA lentivirus packaging used the 2nd generation system. For transfection, 293T cells cultured to 80% confluence were used; lentiviral, packaging (pHelper 1.0; Shanghai GeneChem Co., Ltd.) and envelope (pHelper 2.0; Shanghai GeneChem Co., Ltd.) plasmids were co-transfected at a 4:3:2 molar ratio (total DNA: 45 μg) using GeneChem Transfection Reagent (Shanghai GeneChem Co., Ltd.) at 37˚C for 6 h, and viral supernatants were collected at 72 h post-transfection. Siha cells were infected at a MOI of 20, with medium replaced 12 h post-infection. Stable cell lines were then obtained by puromycin screening; 72 h post-infection, fluorescent protein expression was assessed under a fluorescence microscope, and when fluorescent cells reached ~30%, they were cultured for another 48 h before screening with 2 μg/ml puromycin. The medium was changed every 24 h during screening, and the same puromycin concentration was maintained for subsequent cultures. Stable cell pools were ready for downstream experiments 1 week after screening initiation. The knockdown efficiency of shRNAs was evaluated by reverse transcription-quantitative PCR (RT-qPCR), demonstrating significant downregulation of both HPV16 E7 and HTRA1 expression (Fig. S1A and B).

The sequences of the shRNAs, which are presented in the 5'-3' direction, were as follows: HPV16 E7 shRNA, TGCGTACAAAGCACACACGTA; HTRA1 shRNA, GGGTCTGGGTTTATTGTGT; shRNA negative control, TTCTCCGAACGTGTCACGT.

Transmission electron microscopy. NHEKs ($6x10^6$) were harvested without rinsing and immediately suspended in electron microscope fixative (cat. no. BP006; BIOSSCI). After 5 min, cells were scraped unidirectionally, centrifuged at 1,000 x g for 10 min, resuspended in 1 ml fresh fixative at room temperature, and stored at 4˚C. For agar pre-embedding, the pellet was centrifuged at 1,200 x g for 5 min, washed three times with 0.1 M phosphate buffer (pH 7.4), then mixed with warm 1% agarose and embedded using forceps before solidification. Post-fixation, the samples were incubated with 1% osmium tetroxide (cat. no. 02602-AB; Ted Pella, Inc.) in 0.1 M phosphate buffer (pH 7.4) for 2 h in the dark at room temperature, followed by three 15-min buffer washes. Dehydration was performed using a graded series of ethanol (30, 50, 70, 80 95 and 100%; 10 min each), followed by two 10-min acetone changes, all at room temperature. Subsequently, infiltration and embedding were performed. A mixture of acetone and 812 (cat. no. 02660-AB; SPI Supplies) embedding agent in a 1:1 ratio was used to treat the samples at 37˚C for 3h, followed by a 1:2 mixture at 37˚C overnight. Finally, pure 812 embedding agent was used to treat the samples at 37˚C for 6 h. The pure 812 embedding agent was poured into the embedding plate, the sample was inserted and the plate was incubated at 37˚C overnight. The next step was polymerization, where the embedding plate was placed in a 60˚C oven for 48 h, and the resin blocks were removed for later use. Ultra-thin sectioning was then performed, with the resin blocks being cut into 70-nm sections on an ultrathin sectioning machine and collected on 200 mesh copper grids. Finally, staining was carried out by placing the copper grids in 2% uranyl acetate (cat. no. 02624-AB; Ted Pella, Inc.) saturated alcohol solution for 10 min at room temperature in the dark, followed by three washes with ultrapure water. The grids were then stained with 2% lead citrate solution for 10 min at room temperature in the absence of CO_2, washed three times with ultrapure water, and slightly dried with filter paper. The copper grid sections were placed in a copper grid box and dried at room temperature overnight, and were then observed under a transmission electron microscope (HT7700; Hitachi, Ltd.).

Generation and identification of HTRA1(-/-) mice. HTRA1 gene knockout mice (cat. no. S-KO-10732; strain no. KOCMP-56213-Htra1-B6N-VA) and wild-type (WT) mice (cat. no. C001072; strain no. C57BL/6NCya) were procured from Cyagen Biosciences Inc. The genotype verification process for HTRA1(-/-) mice was performed as follows: The toe tissue of 7-day-old WT and HTRA1(-/-) mice (n=20 mice/group) was cut without anesthesia. These mice were housed together with their respective dams and separately from other adult animals to prevent interference and ensure individual monitoring. Mouse toe tissue was collected in a labeled microcentrifuge tube for DNA extraction, followed by the addition of 100 μl 0.05 mol/l NaOH, incubation at 95˚C for 45 min, neutralization with 30 μl 0.1 mol/l Tris-HCl (pH 8.0), centrifugation at 10,000 x g for 5 min at room temperature, and transfer of the supernatant to a new tube for PCR. PCR was performed using Taq Plus Master Mix II (cat. no. P213-01; Vazyme Biotech Co., Ltd.) under the following conditions: 94˚C for 3 min (1 cycle), followed by 35 cycles of 94˚C for 30 sec, 60˚C for 35 sec and 72˚C for 35 sec, and a final extension step at 72˚C for 5 min (1 cycle). For electrophoresis, a 1.5% agarose gel was prepared in 1X TAE buffer containing ethidium bromide (0.5 μg/ml); subsequently, PCR products and a DNA marker were loaded, the gel was run at 100-20 V for 25-30 min, and finally the bands were visualized under UV light, images were captured and band patterns were analyzed for genotyping (Fig. S1D). The specific verification primer sequences (presented in a 5'-3 'direction) were as follows: WT,

forward (F) CTAGGTGATAGCGGTGGAAGTC, reverse (R) ACAAGTGTATCTGGGCTTCCTG, target band size, 504 bp; HTRA1(-/-), F CAATGGACGAGCCCTGTATCA ATC, R CACTGACTGCTTTTCCAGAGGTCC, target band size, 349 bp.

For subsequent experiments, 8-week-old mice WT and HTRA1(-/-) mice were used (previously genotyped at 7 days of age). Each experimental group consisted of 10 male (weight, 26.1±1.2 g) and 10 female (weight, 20.5±1.2 g) mice. All mice, including neonates, were housed under the following controlled environmental conditions: Temperature, 20-26˚C; relative humidity, 40-70%; 12-h light/dark cycle (lights on from 7:00 AM to 7:00 PM). The bedding consisted of dust-free and absorbent wood shavings. Ventilation was maintained to ensure adequate air exchange and removal of harmful gases, while minimizing direct airflow and noise exposure. Standard laboratory chow and water were provided *ad libitum*. Animals were monitored daily for general health and behavior, and observations were systematically recorded.

WT and HTRA1(-/-) C57BL/6NCya mice at 8 weeks of age were humanely euthanized in accordance with institutional animal care guidelines, and tissue RNA was isolated and submitted for RNA-seq analysis.

Methods of mouse anesthesia and euthanasia. To comply with animal welfare guidelines and reduce unnecessary suffering, predefined humane endpoints were applied to HTRA1(-/-) and WT mice during tissue collection: Mice were immediately euthanized before severe distress occurred if they showed pre-sampling signs such as involuntary vocalization, an inability to maintain a normal posture, severe dehydration (sunken eye sockets, loss of skin elasticity), refusal to eat/drink for >24 h or unexpected skin pathologies (ulceration, bleeding, unrelated inflammation); if anesthesia was inadequate (purposeful movement, vocalization during sampling); or re-anesthesia failed. In the present study, no mice met the criteria for humane endpoints and therefore none were euthanized before the end of the experiment. For anesthesia, the dosage of 5% chloral hydrate was used based on the individual body weight of each mouse, and administered at a standardized concentration of 300 mg/kg. Following physical restraint, the anesthetic was injected into the lower abdominal region via a lateral abdominal approach. Following anesthesia, mouse ears were surgically excised using sterile scissors for subsequent IHC analysis, and euthanasia was performed by cervical dislocation immediately after tissue collection. All procedures adhered to the 3Rs principle and AVMA Guidelines for the Euthanasia of Animals (47,48).

Total RNA sequencing (RNA-seq) analysis. Transcriptomics analysis was conducted on Siha cells with HPV16 E7 gene knockdown, and also on the skin of HTRA1(-/-) mice. Briefly, total RNA was extracted from the samples with TRIzol® reagent (cat. no. 15596026CN; Invitrogen; Thermo Fisher Scientific, Inc.). Only high-quality samples (OD260/280, 1.8-2.2; OD260/230, ≥2.0; RNA quality number, ≥6.5; 28S:18S, ≥1.0; >1 μg) were chosen following quality checks on a 5300 Bioanalyzer (Agilent Biotechnologies, Inc.) and quantification on an ND-2000 (NanoDrop; Thermo Fisher Scientific, Inc.). For library construction, 1 μg total RNA was used to isolate and fragment mRNA via oligo(dT) beads, after which, double-stranded cDNA was synthesized (SuperScript Kit; Thermo Fisher Scientific, Inc.), and processed for end repair, phosphorylation to enable efficient ligation with sequencing adapters (catalyzed by T4 polynucleotide kinase to add 5'-phosphate groups using ATP) and 3'-end 'A' addition to cDNA fragments. Subsequently, 300-bp cDNA fragments were selected, amplified by PCR (15 cycles; Phusion Polymerase; Thermo Fisher Scientific, Inc.), quantified (Qubit 4.0; Thermo Fisher Scientific, Inc.) and sequenced. Paired-end sequencing with a read length of 150 bp (2x150 bp) was performed on the NovaSeq X Plus platform (Illumina, Inc.) using the NovaSeq X Plus Reagent Kit (300 cycles; cat. no. 20104705; Illumina, Inc.), consistent with the reagents typically used by Meiji Biomedical Technology Co., Ltd. for NovaSeq X Plus-based sequencing services. The final library was loaded at a concentration of 15 pM. Molar concentration was determined using the KAPA Library Quantification Kit (cat. no. 07960140001; Roche Diagnostics) via qPCR, ensuring accurate loading for the NovaSeq X Plus platform. Raw reads were trimmed/quality-controlled using fastp (v0.19.5; https://github.com/OpenGene/fastp) (49) to obtain clean reads, which were aligned to the reference genome with HISAT2 (v2.1.0; https://daehwankimlab.github.io/hisat2/) (50) and assembled by StringTie (v2.1.2; https://ccb.jhu.edu/software/stringtie/) (51). Transcript expression (transcripts per million) and gene abundance (RSEM) were calculated, and differentially expressed genes (DEGs) were identified via DESeq2 (v1.24.0; https://bioconductor.org/packages/stats/bioc/DESeq2/) (52) (|log2FC|≥1, FDR≤0.05) or DEGseq (v1.38.0; https://www.rdocumentation.org/packages/DEGseq/versions/1.26.0) (53) (|log2FC|≥1, FDR≤0.001). Gene Ontology (GO) (Goatools; v0.6.5; https://github.com/tanghaibao/goatools) (54) and Kyoto Encyclopedia of Genes and Genomes (KEGG) (KOBAS; v2.1.1; http://bioinfo.org/kobas/download/) (55) enrichment analyses were performed for DEGs (Bonferroni-corrected P≤0.05) using Goatools and KOBAS, respectively. Heatmaps were generated using the Weighted Gene Co-expression Network Analysis (v1.63; https://cran.r-project.org/package=WGCNA) (56). Finally, alternative splicing events were identified via rMATS (v4.0.2; http://rnaseq-mats.sourceforge.net/) (57) (focusing on reference-similar isoforms or novel junctions, detecting exon inclusion/exclusion, alternative 5'/3' ends and intron retention). The RNA-seq analysis was performed by Meiji Biomedical Technology Co., Ltd.

Isobaric tags for relative and absolute quantitation (iTRAQ) analysis. iTRAQ analysis was performed on Siha cells with stable HPV16 E7 knockdown. At ~70% confluence, cells were washed 2-3 times with ice-cold PBS, detached with 0.25% trypsin (cat. no. V5117; Promega Corporation), centrifuged at 800-1,000 x g for 5 min at 4˚C, and washed once more with PBS. Cell pellets were then resuspended in SDT lysis buffer (4% SDS, 100 mM Tris-HCl, pH 7.6; 100-200 μl per 1x10^6 cells), vortexed, sonicated on ice (200-300 W, 3 sec pulse/5 sec interval, 10-15 cycles), and boiled at 95˚C for 15 min. After centrifugation at 14,000 x g for 15 min at 4˚C, the supernatants were quantified using a bicinchoninic acid (BCA) kit (cat. no. P0012; Beyotime Institute of Biotechnology) and stored at -20˚C. For SDS-PAGE validation, 20 μg protein was mixed

with 6X loading buffer, denatured at 95˚C for 5 min, separated on a 12% gel (250 V, 40 min), and stained with Coomassie Brilliant Blue. For iTRAQ processing, 150 μg protein was reduced with 100 mM DTT (cat. no. 43819-5G; Sigma-Aldrich; Merck KGaA) at 95˚C for 5 min, transferred to a 30 kDa filter, washed with UA buffer (8 M urea, 150 mM Tris-HCl, pH 8.5), alkylated with 50 mM IAA (cat. no. I1149-5G; Sigma-Aldrich; Merck KGaA) in the dark for 30 min, and washed with 25 mM NH_4HCO_3 (cat. no. A6141-25G; Sigma-Aldrich; Merck KGaA). Digestion was performed overnight at 37˚C with 4 μg trypsin (substrate:enzyme 37.5:1) in NH_4HCO_3. Peptides were collected, desalted, lyophilized, reconstituted in 0.1% formic acid (cat. no. A117; Thermo Fisher Scientific, Inc.), and quantified by measuring the absorbance at a wavelength of 280 nm. The peptides were separated using a nanoflow liquid chromatography system (Easy nLC; Thermo Fisher Scientific, Inc.) on an Acclaim™ PepMap™ RSLC analytical column (50 μm x 15 cm, NanoViper; cat. no. 164943; Thermo Fisher Scientific, Inc.) with 0.1% formic acid/water-acetonitrile gradients (elution times of 1/2/3 h; flow rate, 300 nl/min). The peptides were analyzed on a Q Exactive Plus mass spectrometer (Thermo Fisher Scientific, Inc.) operated in positive mode with a resolution of 70,000 for mass spectrometry scans and higher-energy collisional dissociation for fragmentation. This experiment adopted a non-targeted proteomics analysis strategy with full scan combined with MS2 fragmentation. The nitrogen gas parameters used were: A temperature of 300˚C, a nebulizer pressure of 40 psi and a flow rate of 7 l/min, which were fully compatible with the experimental process. Raw data were processed with Proteome Discoverer 2.1 (https://thermo.flexnetoperations.com/control/thmo/login?nextURL=%2Fcontrol%2Fthmo%2Fhome) (58) to generate.mgf files, searched against the UniProt human database (https://www.uniprot.org/) (59) via MASCOT 2.6 (https://www.matrixscience.com//server.html) (45), and filtered for FDR<0.01 to obtain results.

GFP-LC3 and Mito-Tracker Red CMXRos colocalization. A GFP-LC3 plasmid (1 μg/ml; cat. no. 17-10193; Sigma-Aldrich; Merck KGaA) was transfected into HPV11/16 E7-overexpressing cells at 37˚C for 6 h using liposome transfection reagent (Lipofectamine® 3000; Invitrogen, Thermo Fisher Scientific, Inc.) according to the manufacturer's protocol. After the 6-h transfection, the culture medium was replaced with fresh medium, and the cells were continuously cultured under the same conditions (37˚C, 5% CO_2). At 36 h post-transfection, the cells were stained with 100 nM Mito-Tracker Red CMXRos (cat. no. C1035; Beyotime Institute of Biotechnology) for 20 min at room temperature followed by instant observation. The number of all punctate granules and yellow punctate granules within the cells was quantified using a fluorescence microscope. For each sample, 100 cells were observed. After computing the ratio of yellow punctate granules to all punctate granules, the mean value of the data was obtained, and intergroup comparisons were carried out. A higher proportion of yellow punctate granules indicated enhanced mitophagy.

Western blot analysis. Cells were collected and lysed in radioimmunoprecipitation assay lysis buffer (containing 1% phenylmethylsulfonyl fluoride; Fdbio Science) for 30 min on ice. The lysates were centrifuged at 10,000 x g for 20 min at 4˚C, and the supernatants were collected. The supernatants were then harvested and the protein concentrations were quantified using a BCA kit. Since HTRA1 is an exosomal protein, when determining the expression levels of HTRA1, intracellular and extracellular proteins need to be assessed simultaneously (60,61). Firstly, for extracellular lysate extraction, the cell culture medium was collected, and an equivalent volume of methanol was added and mixed thoroughly, after which, 1/3 volume of chloroform was added and the sample was vortexed. Subsequently, the mixture was centrifuged at 10,000 x g for 10 min at 4˚C and liquid stratification could be observed. Upon carefully removing the uppermost layer of liquid (being cautious to avoid disturbing the thinner protein middle layer), 500 μl methanol was added. After thorough vortexing, the mixture was centrifuged at 10,000 x g for 10 min at 4˚C. Subsequently, the upper layer of liquid was removed (being careful to avoid disturbing the extracellular lysate protein at the bottom layer) and the protein was incubated at 55˚C for 5 min. The volume of the intracellular and extracellular lysates was kept consistent.

After protein extraction, the protein samples (10 μg/lane) were separated by SDS-PAGE on 12% gels and were subsequently transferred onto polyvinylidene fluoride membranes (0.2 μm; cat. no. 1620177; Bio-Rad Laboratories, Inc.) using a wet transblotting apparatus (Bio-Rad Laboratories, Inc.). Upon blocking with 10% nonfat milk (Difco; BD Biosciences) for 1 h at room temperature, the membranes were incubated overnight with the following primary antibodies diluted to 1:1,000 in primary antibody diluent (cat. no. FD0040; Hangzhou Fude Biological Technology Co., Ltd.): Mitophagy Antibody Sampler kit (cat. no. 43110; Cell Signaling Technology, Inc.), polyclonal rabbit anti-HTRA1 (cat. no. SAB1300009; Sigma-Aldrich; Merck KGaA), polyclonal rabbit anti-LC3B (cat. no. L8918; Sigma-Aldrich; Merck KGaA), monoclonal mouse anti-GAPDH (cat. no. G8795; Sigma-Aldrich; Merck KGaA), monoclonal rabbit anti-p62 (cat. no. ab109012; Abcam), anti-Flag (cat. no. M1403-2; HUABIO), polyclonal rabbit anti-HPV11/16 E7 (prepared in our laboratory) (62-65) and monoclonal rabbit anti-pRB (cat. no. ab181616; Abcam). After washing the membranes three times with PBS (10 min each), they were incubated for 2 h at room temperature with horseradish peroxidase (HRP)-conjugated goat anti-rabbit IgG (H+L; cat. no. A0208; Beyotime Institute of Biotechnology) or HRP-conjugated goat anti-mouse IgG (H+L; cat. no. A0216; Beyotime Institute of Biotechnology) secondary antibodies diluted to 1:500 in 5% skimmed milk. The specific protein bands were detected with enhanced chemiluminescence reagents (cat. no. FD8020; Hangzhou Fude Biological Technology Co., Ltd.) using a blot scanner (v2.3; ChemiDoc Touch; Bio-Rad Laboratories, Inc.). ImageJ (version 1.54f; National Institutes of Health) was used for image processing and semi-quantitative analysis.

RT-qPCR. The relative gene expression levels were measured by RT-qPCR. Total RNA was extracted from cells using TRIzol reagent. First-strand cDNA was synthesized using the PrimeScript™ High Fidelity RT-PCR Kit (cat. no. R022A; Takara Bio, Inc.) according to the manufacturer's protocol. The relative gene expression levels were measured by qPCR in a total volume of 10 μl including 1 μl cDNA, 5 μl 2X SYBR

Premix Ex Taq I (cat. no. RR390A; Takara Bio, Inc.), 0.4 μl forward primer, 0.4 μl reverse primer, 0.2 μl carboxy-X-rhodamine and 3 μl double-distilled H_2O run on an ABI 7500 system (Applied Biosystems; Thermo Fisher Scientific, Inc.). qPCR was carried out in 96-well plates at 95˚C for 2 min, followed by 40 cycles at 95˚C for 10 sec and 58˚C for 30 sec. Relative gene expression levels were calculated using the $2^{-\Delta\Delta Cq}$ method, with GAPDH as the reference gene to normalize the expression of target genes (66). The primer sequences (presented in the 5'-3' direction) were as follows: HTRA1, F TCCCAACAGTTT GCGCCATAA,R CCGGCACCTCTCGTTTAGAAA; IFN-β, F AACTGCAACCTTTCGAAGCCTTT, RAGAGCAATTTG GAGGAGACACTT; HPV16 E7, F CCGGACAGAGCCCAT TACAA, R TTTGTACGCACAACCGAAGC; HPV11 E7, F GATGTGACAGCAACGTCCGA, R GTGTGCCCAGCA AAAGGTCT; PODXL, F CTCCCTGCTAGACCTCCTG, R TGCAGAATCCGAGACTCTTCAT; CEBPD, F CTGTCG GCTGAGAACGAGAA, R TCTTTGCGCTCCTATGTCCC; S10A6, F CTCCCTACCGCTCCAAGC, R CACCTCCTG GTCCTTGTTCC; ANXA8, F ATGGCCTGGTGGAAATCC TG, R TCATGCTGCTGAGGGTCTTG; GAPDH, F CTC ACCGGATGCACCAATGTT, R CGCGTTGCTCACAAT GTTCAT.

Clinical samples. The inclusion criteria for patients with condyloma acuminatum were as follows: Male participants, aged 18-45 years (mean ± SD, 30.9±4.8 years; median, 30 years); clinically confirmed condyloma acuminatum with HPV11 PCR positivity; absence of comorbidities; and no prior HPV vaccination. The exclusion criteria in the patient group were as follows: Other HPV types except for HPV11 detected by PCR; those with any history of HPV vaccination; individuals with mental illness, cognitive impairments or critical illnesses; or minors. The inclusion criteria for the participants in the healthy control group were: Male participants, aged 18-45 years (mean ± SD, 29.8±4.5 years; median, 30 years); normal foreskin tissue, with no evidence of HPV infection; and no prior HPV vaccination. The exclusion criteria in the control group were as follows: Detection of HPV via PCR; prior HPV vaccination; and individuals with mental illness, cognitive impairments or critical illnesses; or minors. Condyloma acuminatum and normal foreskin tissue samples were utilized for immunohistochemical analysis, with 15 cases enrolled in each group.

The inclusion criteria for patients with cervical cancer were as follows: Female participants, aged 18-45 years (mean ± SD, 31.6±4.9 years; median, 31 years); clinically confirmed cervical cancer with HPV16 PCR positivity; absence of comorbidities; and no prior HPV vaccination. The exclusion criteria in the patient group were as follows: Other HPV types except for HPV16 detected by PCR; those with any history of HPV vaccination; pregnant women; individuals with mental illness, cognitive impairments or critical illnesses; or minors. The inclusion criteria for the participants in the control group were: Female participants, aged 18-45 years (mean ± SD, 30.9±4.8 years; median, 31 years); clinically confirmed cervical cancer but a negative HPV test; and no prior HPV vaccination. The exclusion criteria for the control group were as follows: Detection of HPV via PCR; prior HPV vaccination; pregnant women; individuals with mental illness, cognitive impairments or critical illnesses; or minors. Cervical cancer tissues positive for HPV16 ($HPV16^{+}$) or negative for HPV (HPV^{-}) were used for immunohistochemical analysis, with 15 cases in each group.

Immunohistochemistry (IHC). Tissue samples (condyloma acuminatum and normal foreskin tissues, HPV^{-} and $HPV16^{+}$ cervical cancer tissues, and mouse ear tissues) were collected and fixed in 4% formaldehyde (cat. no. BL539A; Biosharp Life Sciences) at room temperature for 48 h. Subsequently, the samples were paraffin-embedded and sectioned (3-4 μm). The sections were then incubated in an oven at 60˚C for 2 h, and subsequently underwent dewaxing and hydration processes. To inhibit endogenous peroxidase activity, 1% hydrogen peroxide dissolved in methanol was added to the slides, followed by antigen retrieval through high-pressure heat repair. Subsequently, 10% goat serum (Beyotime Institute of Biotechnology) was added to block non-specific antigens, followed by incubation at room temperature (~25˚C) for 30 min. The goat serum was removed from the sections, and the corresponding primary antibodies [anti-HPV11/16 E7, 1:500, prepared in our laboratory (62-65); or anti-HTRA1, 1:1,000, cat. no. 55011-1-AP, Proteintech Group, Inc.] were added, followed by incubation at room temperature for 1 h. After cleaning, a polymer enhancer was applied and incubated at room temperature for 15 min, and a HRP-labeled secondary antibody (goat anti-rabbit IgG; 1:500; cat. no. A0208; Beyotime Institute of Biotechnology) was added and incubated at room temperature for 30 min prior to DAB color development. The color developing solution was prepared by mixing 1 ml diluent with 40 μl DAB stock solution. The durations for color development were ~1 min for HPV11/16 E7 and ~30 sec for HTRA1. The reaction was promptly terminated with tap water to prevent excessive color development. Subsequently, hematoxylin counterstaining, ethanol dehydration, xylene dewaxing and neutral gum sealing were carried out, and images were captured using an inverted light microscope (IX83; Olympus Corporation). The IHC results in the present study were assessed using a semi-quantitative scoring system. Briefly, scores were assigned independently based on staining intensity and the percentage of positive cells, with the final score calculated as the product of these two values. Staining intensity was scored as follows: 0, no detectable staining; 1, light yellow staining, 2, yellow staining; and 3, brown staining. The percentage of positive cells was scored as follows: 1, ≤25%; 2, 26-50%; 3, 51-75%; and 4, >75%.

Construction of truncated plasmids. Based on the functional domain architecture of the HTRA1 protein, three truncated mutants were designed, namely IB [deletion (del) 35-111 aa], KAZAK (del 115-155 aa) and PDZ (del 382-480 aa). Each target gene fragment was synthesized via full-gene synthesis and subsequently cloned into Flag-tagged expression vectors (cat. no. GV657: Shanghai GeneChem Co., Ltd.). The control group was transfected with the CMV enhancer-MCS-polyA-EF1A-zsGreen-sv40-puromycin plasmid vector (cat. no. GV658; Shanghai GeneChem Co., Ltd.). Briefly, 5 μl recombinant plasmids were mixed with 50 μl chemically competent DH5α cells (cat. no. 9057; Takara Bio, Inc.) and incubated on ice for 30 min. The mixture was heat-shocked at 42˚C

for 90 sec, followed by immediate cooling on ice for 2 min. Subsequently, 500 μl pre-warmed Luria-Bertani (LB) medium (cat. no. L8291; Beijing Solarbio Science & Technology Co., Ltd.) without antibiotics was added, and the cells were shaken at 37˚C for 1 h to allow recovery and expression of the antibiotic resistance gene. An aliquot of the transformation mixture was plated onto LB agar plates containing ampicillin, which were then incubated inverted at 37˚C for 12-16 h. Subsequently, 5-10 single colonies were selected and inoculated into 50 μl liquid LB medium supplemented with ampicillin. Cultures were incubated at 37˚C with shaking for 2-3 h and 2 μl of each culture was used directly as a template in colony PCR amplification. A single bacterial colony was aseptically picked using a sterile pipette tip and transferred into a 20-μl identification reaction mixture. The mixture was gently homogenized by pipetting and immediately subjected to PCR amplification. The 20 μl reaction system consisted of 9 μl ddH_2O, 10 μl 2X Taq Plus Master Mix, 0.5 μl forward primer (10 μM), 0.5 μl reverse primer (10 μM) and the single colony as the template. Thermal cycling conditions were as follows: Initial denaturation at 95˚C for 5 min, followed by 22 cycles of denaturation at 95˚C for 30 sec, annealing at 56˚C for 30 sec and extension at 72˚C for 1 min per kb, with a final extension step at 72˚C for 8 min. PCR products were analyzed by 1% agarose gel electrophoresis, and clones exhibiting the expected band size [(IB (del 231 bp), KAZAK (del 123 bp) and PDZ (del 87 bp)] were considered positive. Plasmids from positive clones were extracted and subjected to Sanger sequencing. The obtained sequences were aligned with the reference target gene sequence to confirm the correct insertion and absence of mutations, deletions, or insertions, thereby completing the validation of the recombinant plasmid. Following sequence confirmation [IB (del 35-111 aa), KAZAK (del 115-155 aa) and PDZ (del 382-480 aa)], the verified clones were cultured for plasmid amplification, and high-purity plasmid DNA was extracted. The extracted plasmids (1 μg/well for 6-well plates) were then transfected into HPV11/16 E7-overexpressing 293T cells, which were seeded at a density of $5x10^5$ cells/well in 6-well plates (70-80% confluence), using Lipofectamine 3000 according to the manufacturer's protocol. The transfection was performed at 37˚C for 6 h in a humidified incubator with 5% CO_2. After the 6-h transfection, the culture medium was replaced with fresh medium, and the cells were continuously cultured under the same conditions (37˚C, 5% CO_2). The cells were harvested for subsequent co-immunoprecipitation (CO-IP) assays at 48 h post-transfection.

Immunofluorescence assay. Cells (30% confluence) were fixed with 4% paraformaldehyde (Bio-Rad Laboratories, Inc.) for 15 min at room temperature. For immunofluorescence assays, the cells were then permeabilized with 0.1% Triton X-100 (Beijing Solarbio Science & Technology Co., Ltd.) for 10 min. Next, the fixed permeabilized cells were blocked with 10% goat serum containing 1% bovine serum albumin (cat. no. 15260037; Gibco; Thermo Fisher Scientific, Inc.) for 60 min at room temperature, and incubated overnight at 4˚C with polyclonal rabbit anti-HTRA1 IgG (1:100; cat. no. 55011-1-AP; Proteintech Group, Inc.). The cells were subsequently incubated with Alexa Fluor 555-conjugated donkey anti-rabbit IgG (1:500; cat. no. 711-565-152; Beyotime Institute of Biotechnology) for 2 h in the dark. Finally, the cell nuclei were stained with DAPI (1:1,000; Beyotime Institute of Biotechnology) for 10 min at room temperature, and images were obtained under a Zeiss fluorescence microscope (Carl Zeiss AG).

CO-IP. HPV11/16 E7-overexpressing NHEKs were cultured under optimal conditions prior to subsequent CO-IP. In addition, 293T cells were cultured to 60-80% confluence and then infected with lentiviruses expressing HPV11/16 E7 protein. Subsequently, the HPV11/16 E7-overexpressing 293T cells were further cultured to 60-80% confluence, and then transfected with truncated HTRA1 plasmids (IB, KAZAK and PDZ, respectively) as aforementioned. The cells were then incubated at 37˚C. After 48 h of culture, the cells were harvested for subsequent experiments. Cells were harvested and lysed in radioimmunoprecipitation assay lysis buffer containing 1% phenylmethylsulfonyl fluoride (Fdbio Science) for 30 min. Following centrifugation at 10,000 x g for 20 min at 4˚C, the supernatants were collected, and protein concentrations were determined using a BCA protein assay kit. Protein A/G magnetic beads (50 μl; cat. no. 36417ES03; Shanghai Yeasen Biotechnology Co., Ltd.) were first transferred to a 1.5-ml tube, placed on a magnetic separation rack (cat. no. FMS012; Beyotime Institute of Biotechnology) for 30 sec, and the storage buffer was then carefully removed. The beads were washed three times with 500 μl ice-cold weak RIPA lysis buffer (cat. no. P0013D; Beyotime Institute of Biotechnology). Antibody coupling was performed by adding 2 μg of either Flag antibody, E7 antibody or control IgG antibody to the beads, bringing the total volume to 300 μl with weak RIPA buffer, and incubating the suspensions at 4˚C with end-over-end rotation for 2 h to allow formation of the antibody-bead complexes. Subsequently, 500 μl cell lysate, which was pre-adjusted to 2 mg/ml total protein, was added to each antibody-conjugated bead preparation, and the mixtures were rotated overnight at 4˚C to capture the target proteins. The next day, the tubes were placed on the magnetic rack, the supernatants were discarded and the beads were subjected to five stringent washes with 1 ml ice-cold weak RIPA buffer per wash. After the final wash, 50 μl 1X SDS loading buffer was added to each bead pellet, the suspensions were vortexed thoroughly, heated at 100˚C in a metal block for 10 min to elute the immunocomplexes, and then chilled on ice for 2 min. The tubes were briefly centrifuged at 12,000 x g for 30 sec, returned to the magnetic rack and the clarified supernatants were carefully transferred to fresh tubes for subsequent western blot analysis. The IgG control antibodies used in this process included Normal Rabbit IgG (cat. no. 30000-0-AP; Proteintech Group, Inc.) and Normal Mouse IgG (cat. no. B900620; Proteintech Group, Inc.), polyclonal mouse anti-Flag (tag for truncated plasmids, cat. no. M1403-2; HUABIO) and polyclonal rabbit anti-HPV11/16 E7 (prepared in our laboratory). Given that both high-risk and low-risk HPV E7 proteins are well established to interact with pRB (9,10), the specificity of HPV11/16 E7 antibodies in NHEKs overexpressing HPV11/16 E7 were validated using a CO-IP assay followed by detection of pRB; the results demonstrated that HPV11/16 E7 antibodies effectively captured and co-precipitated pRB, confirming their functional utility (Fig. S1E).

ELISA. To evaluate the levels of IFN-β secreted by NHEKs with overexpression of HPV11/16 E7 and knockdown of HTRA1, the IFN-β ELISA kit (cat. no. E-EL-H0085; Elabscience; Elabscience Bionovation Inc.) was used. Cell supernatants were collected by centrifugation at 1,000 x g for 15 min at 4˚C and stored at -20˚C until analysis. The assay was conducted according to the manufacturer's instructions. Optical density (OD) values were measured within 5 min using a microplate reader set at a reference wavelength of 630 nm and a detection wavelength of 450 nm. The OD value of the blank well was subtracted from all other well readings (duplicate wells were averaged). A standard curve was generated by plotting the mean OD values against the known standard concentrations, and a four-parameter logistic regression model was applied for curve fitting. The concentrations of IFN-β in the samples were interpolated from the standard curve and multiplied by the respective dilution factors to obtain the final concentrations.

Statistical analysis. Data, with the exception of IHC results, are presented as the mean ± standard deviation. Significant differences between groups were determined by one-way ANOVA with Tukey's honestly significant difference post hoc test. IHC data are presented as median values with interquartile range, and statistical analysis of IHC data was performed using the Mann-Whitney U test. $P<0.05$ was considered to indicate a statistically significant difference.

Results

HPV E7 promotes mitophagy in keratinocytes. Transmission electron microscopy was used to observe the number of mitochondrial autophagosomes in the control group and in NHEKs overexpressing HPV11/16 E7 (Fig. 1A). The results demonstrated that there were more mitochondrial autophagosomes in NHEKs overexpressing HPV11/16 E7 than in control cells. In addition, intracellular mitophagy was monitored via co-localization of GFP-LC3 and Mito-Tracker Red CMXRos (Fig. 1B and C), and it was observed that, compared with that in the control groups, the proportion of yellow puncta was higher in the HPV11/16 E7 overexpression groups, suggesting a higher level of mitophagy in these groups. The expression levels of the mitophagy-related proteins LC3 and p62, as well as the status of the mitophagy-related pathways PINK1/Parkin and BNIP3/BNIP3L were examined by western blotting (Fig. 1D and F). The experimental results indicated that HPV11/16 E7 may activate the PINK1/Parkin and BNIP3/BNIP3L pathways, enhance LC3 expression, suppress p62 expression and consequently promote mitophagy in keratinocytes; however, this phenomenon was inhibited by the mitophagy inhibitor cyclosporine A (cat. no. HY-B0579; MedChemExpress; 5 μmol/l, 12 h, 37˚C) (Fig. 1E and G).

HPV E7 enhances the expression of the HTRA1 gene in keratinocytes. Siha cells with stable knockdown of HPV16 E7 were employed to perform RNA-seq analysis at the transcriptional level and iTRAQ analysis at the protein level. The heatmaps showed significant differences between the control and the knockdown groups (Fig. 2A), and a total of 174 genes exhibiting consistent expression trends and statistically significant alterations in both transcriptomic and proteomic profiles were identified (Fig. 2B). Among these, five potential mitophagy-related genes were selected for further validation based on a comprehensive review of the literature: PODXL (67,68), CEBPD (69,70), HTRA1 (71,72), S10A6 (73,74) and ANXA8 (75,76) (Fig. 2C). RT-qPCR was subsequently performed to assess the expression levels of these genes in the control and knockdown groups. The results demonstrated that PODXL, CEBPD, HTRA1 and S10A6 were significantly downregulated in the knockdown group; notably, HTRA1 exhibited the most pronounced differential expression between the two groups (Fig. 2D). In addition, GO analysis of the RNA-seq data revealed that among the statistically significant GO terms, HTRA1 was involved in multiple GO terms associated with mitophagy (Fig. 2E). For example, GO:0090288 'negative regulation of cellular response to growth factor stimulus (77,78), GO:0090101 'negative regulation of transmembrane receptor protein serine/threonine kinase signaling pathway (79) and GO:0090287 'regulation of cellular response to growth factor stimulus (80) are biological processes closely related to mitophagy.

In addition, compared with in the control group, the expression of HTRA1 was significantly downregulated both intracellularly and extracellular in the 16E7 knockdown group (Fig. 2G and I). Furthermore, a lentivirus was used to stably express HPV11 E7 in NHEKs, and the expression of HTRA1 was subsequently assessed. It was noticed that low-risk HPV11 E7 was capable of facilitating the mRNA and protein expression levels of HTRA1 (Fig. 2F and H). Concurrently, elevated intracellular and extracellular expression of HTRA1 was observed in both $HPV11^+$ condyloma acuminatum tissue specimens and $HPV16^+$ cervical cancer tissue, with normal foreskin tissue and HPV^- cervical cancer tissue samples serving as respective controls.(Fig. 2J and K). Although HTRA1 is primarily recognized as a secreted protein, previous evidence has suggested that it also exhibits intracellular expression (81,82). Immunofluorescence staining revealed detectable levels of HTRA1 within NHEKs (Fig. 2L and M). Furthermore, the group overexpressing HPV11 and HPV16 E7 exhibited a higher expression of HTRA1 compared with that in the control group.

HPV E7 induces mitophagy in keratinocytes through the modulation of HTRA1 gene expression. A lentivirus was used to stably express HPV11/16 E7 in NHEKs and HTRA1 knockdown was subsequently performed. Intracellular mitophagy vesicles were observed by transmission electron microscopy (Fig. 3A). Compared with in the HPV11/16 E7 overexpression group, the number of intracellular mitophagy puncta decreased after knocking down the expression of HTRA1. Intracellular mitophagy was further examined by observing the co-localization of GFP-LC3 and Mito-Tracker Red CMXRos (Fig. 3C and E). It was revealed that the proportion of yellow punctate granules decreased following HTRA1 knockdown in HPV11/16 E7-overexpressing NHEKs, indicating reduced mitophagy activity in the HTRA1 knockdown group. Western blotting was employed to detect the expression levels of the mitophagy-related proteins LC3 and p62, as well as proteins associated with mitophagy pathways (Fig. 3B and D).The results confirmed that following HTRA1 knockdown, the differences in p62 and LC3B expression levels between the control group and the HPV E7 overexpression group were significantly

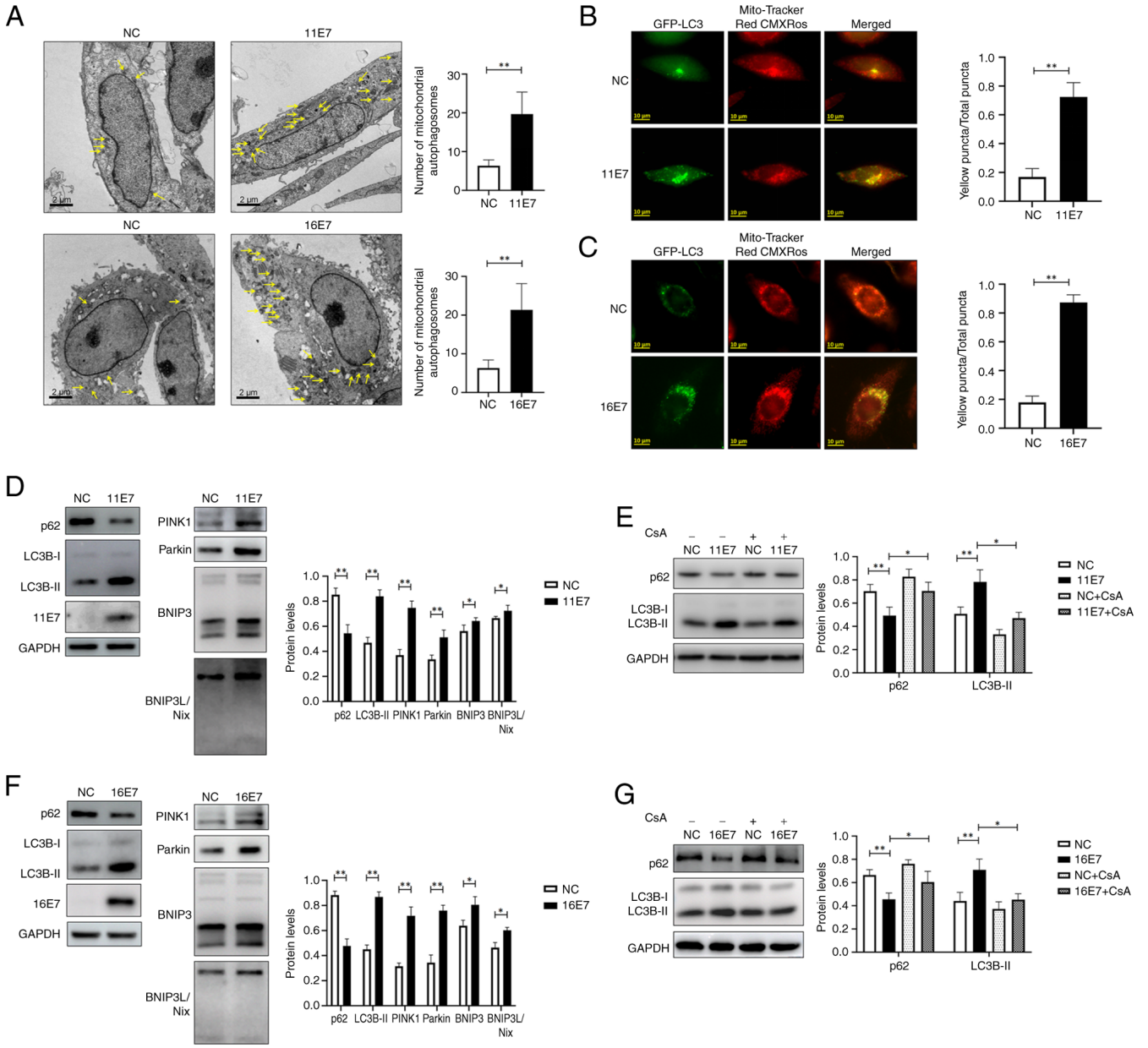

Figure 1. HPV E7 induces mitophagy in keratinocytes (A) Mitophagy in NHEKs overexpressing HPV11/16 E7 was ascertained through transmission electron microscopy. The yellow arrows indicate mitochondrial autophagosomes. The number of mitochondrial autophagosomes was statistically analyzed and a total of 100 cells were analyzed per experiment. Intracellular mitophagy in NHEKs overexpressing (B) HPV11 E7 and (C) HPV16 E7 was analyzed with GFP-LC3 and Mito-Tracker Red CMXRos. The yellow dots indicate co-localized molecules. The ratio of yellow dots to all dots was statistically analyzed and a total of 100 cells were analyzed per experiment. Alterations in mitophagy-related proteins and pathways were detected by western blotting in NHEKs overexpressing (D) HPV11 E7 and (F) HPV16 E7. All proteins were normalized to the loading control GAPDH. Expression levels of mitophagy-related proteins and pathways were investigated in NHEKs overexpressing (E) HPV11 E7 or (G) HPV16 E7 and stimulated with the mitophagy inhibitor CsA. *P<0.05, **P<0.01. BNIP3, Bcl-2 and adenovirus E1B 19 kDa-interacting protein 3; BNIP3L, BNIP3-like; CsA. CsA, cyclosporine A; NC, negative control; HPV, human papillomavirus; NHEK, normal human epidermal keratinocyte; PINK1, PTEN-induced kinase 1.

diminished. Furthermore, the role of HTRA1 in mediating HPV E7-induced activation of the PINK1/Parkin signaling pathway was investigated. The results demonstrated that overexpression of HPV E7 activated this pathway; however, upon HTRA1 knockdown, the difference in PINK1/Parkin pathway activity between the control group and the HPV E7 overexpression group was markedly attenuated; however, changes in BNIP3/BNIP3L were not statistically significant.

Knocking out HTRA1 attenuates mitophagy. HTRA1(-/-) mice were acquired from Cyagen Biosciences Inc. The genotype was detected and verified by agarose gel electrophoresis (Fig. S1D). Subsequently, skin tissue was harvested from 8-week-old WT and HTRA1(-/-) mice, and total RNA was extracted for RNA-seq. The resulting sequences were subjected to heatmap visualization and KEGG signaling pathway analysis (Fig. 4A and B). The findings indicated that HTRA1 was closely associated with the 'Immune system' and 'Infectious disease: viral'. Furthermore, HTRA1 was shown to be closely related with 'Lipid metabolism', 'Signal transduction' and 'Cellular community-eukaryotes'. Subsequently, IHC was applied to evaluate PINK1, Parkin, IFN-β, IL-1β and IL-6

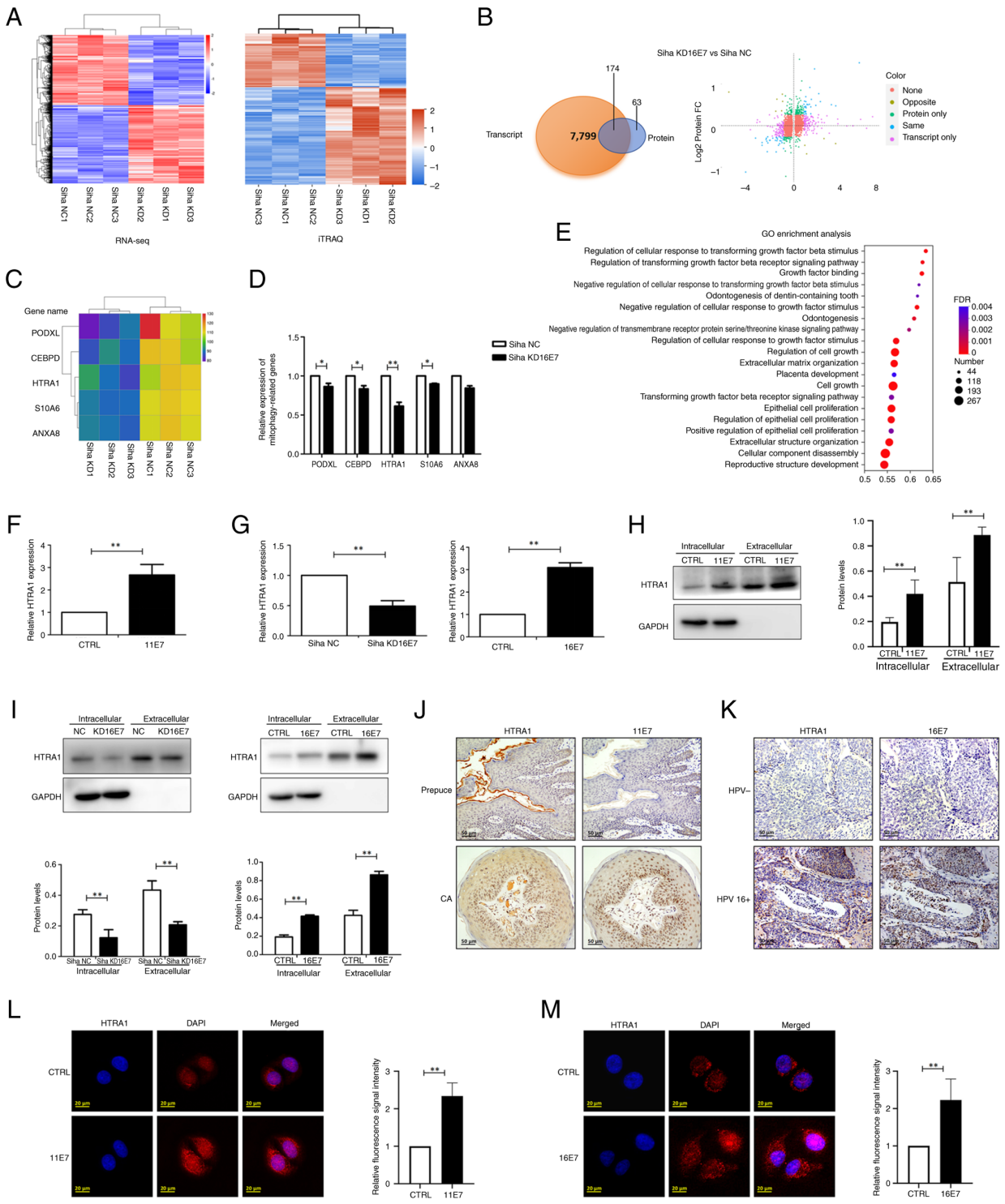

Figure 2. HPV E7 facilitates the expression of HTRA1 within keratinocytes. (A) Heatmap of RNA-seq and iTRAQ analyses. (B) Examination of differentially expressed genes via RNA-seq and iTRAQ analyses. 'None' indicates that there was no difference in the expression of these genes between groups; 'opposite' indicates that the expression trend of the gene was opposite in RNA-seq and iTRAQ analyses; 'same' indicates that the expression trend of the gene was consistent in RNA-seq and iTRAQ analyses; 'transcript only' indicates that these alterations were observed exclusively in the RNA-seq data; 'protein only' indicates that these alterations were observed exclusively in the iTRAQ data. (C) Heatmap presenting the potential genes related to mitophagy derived from the analysis (PODXL, CEBPD, HTRA1, S10A6 and ANXA8). (D) qPCR was used to verify the expression of potential mitophagy-related genes in the HPV16 E7 KD group. (E) GO analysis of RNA-seq data indicated that HTRA1 was significantly enriched in GO terms associated with mitophagy. (F) qPCR was used to detect the expression of HTRA1 in HPV11 E7-overexpressing NHEKs. (G) qPCR was used to detect the expression of HTRA1 in HPV16 E7-overexpressing NHEKs and in stable Siha cells with knockdown of HPV16 E7. (H) Western blotting was used to confirm the expression of intracellular and extracellular HTRA1 in HPV11 E7-overexpressing NHEKs. (I) Western blotting was used to determine the expression of intracellular and extracellular HTRA1 in HPV16 E7-overexpressing NHEK cells and HPV16 E7 KD Siha cells. (J) Examination of the expression of HTRA1 and HPV11 E7 in CA and normal foreskin samples by IHC. (K) Examination of the expression of HTRA1 and HPV16 E7 in HPV-negative cervical cancer and HPV 16-positive cervical cancer tissues by IHC. Intracellular expression levels of HTRA1 protein were assessed and compared between the CTRL group and the (L) HPV11 E7 and (M) HPV16 E7 overexpression groups using immunofluorescence analysis. *P<0.05, **P<0.01. CA, condyloma acuminatum; HPV, human papillomavirus; HTRA1, high-temperature requirement A serine peptidase 1; GO, Gene Ontology; IHC, immunohistochemistry; iTRAQ, isobaric tags for relative and absolute quantitation; NC, negative control; KD, knockdown; NHEK, normal human epidermal keratinocyte; qPCR, quantitative PCR; RNA-seq, RNA sequencing.

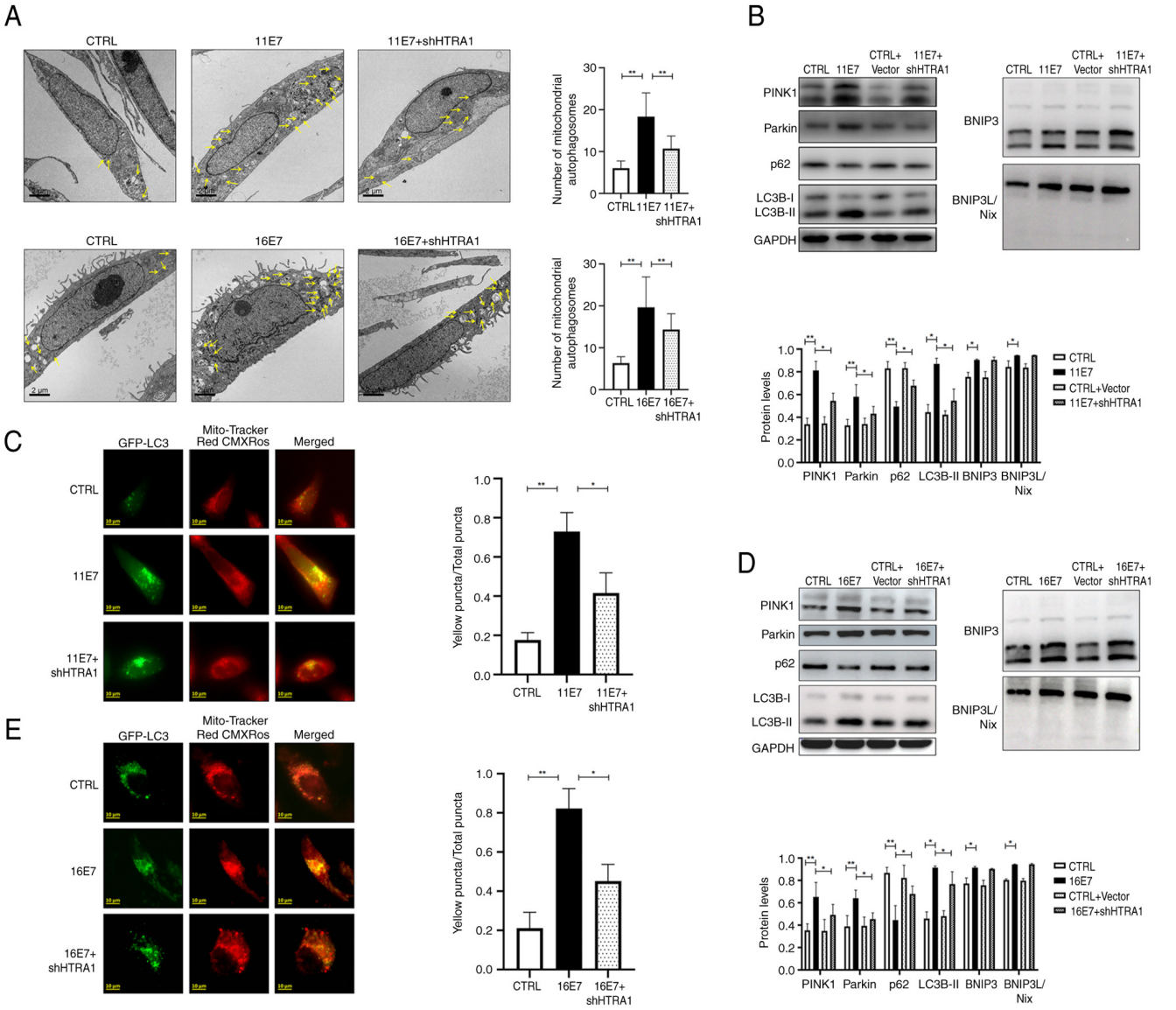

Figure 3. HPV E7 activates mitophagy in keratinocytes through modulating the expression of HTRA1. (A) Transmission electron microscopy was adopted to observe the mitophagy status within HPV11/16 E7-overexpressing NHEKs with HTRA1 knockdown. The yellow arrows indicate mitochondrial autophagosomes. The number of mitochondrial autophagosomes was statistically analyzed and a total of 100 cells were analyzed per experiment. Western blotting was employed to detect the expression of mitophagy-related proteins and pathways in NHEKs with overexpression of (B) HPV11 E7 and (D) HPV16 E7 after HTRA1 knockdown. Co-localization of GFP-LC3 and Mito-Tracker Red CMXRos was employed to observe mitophagy within (C) HPV11 E7-overexpressing and (E) HPV16 E7-NHEKs with HTRA1 knockdown. The yellow dots represent the co-localized areas. The ratio of yellow dots to all dots was calculated and a total of 100 cells were analyzed for each experiment. All proteins were normalized to the loading control GAPDH. *P<0.05, **P<0.01. BNIP3, Bcl-2 and adenovirus E1B 19 kDa-interacting protein 3; BNIP3L, BNIP3-like; CTRL, control; HPV, human papillomavirus; HTRA1, high-temperature requirement A serine peptidase 1; NHEK, normal human epidermal keratinocyte; PINK1, PTEN-induced kinase 1; sh, short hairpin.

expression in the ear tissues of WT and HTRA1(-/-) mice. The results were statistically analyzed using the Mann-Whitney U test and demonstrated downregulation of PINK1 and Parkin expression in the HTRA1(-/-) group, alongside an upregulation of IFN-β expression; however, changes in inflammatory factors such as IL-1β, IL-6 and MCP-1 were not statistically significant (Fig. 4C and D). These results indicated that knockdown of HTRA1 could inhibit the expression of PINK1 and Parkin, while promoting type I IFN production. Subsequently, qPCR and ELISA were employed to assess the expression levels of type I IFNs in HPV11/16 E7-overexpressing NHEKs following HTRA1 gene knockdown. The results demonstrated that the reduced IFN expression levels, induced by HPV E7 overexpression, exhibited partial recovery after HTRA1 knockdown (Fig. 4E). To investigate the functional role of HTRA1, HTRA1 was overexpressed in NHEKs and the expression levels of autophagy-related proteins were assessed using western blot analysis. Western blot analysis indicated that overexpression of HTRA1 alone may promote mitophagy by affecting the expression levels of proteins in the PINK1/Parkin pathway, whereas the expression levels of proteins in the other classic mitophagy-related pathway, BNIP3/BNIP3L, remained unchanged (Fig. 4F). To investigate the regulatory effect of HPV E7 on HTRA1, an IP assay was performed, which confirmed the physical interaction between the two proteins (Fig. 4G). To precisely map the binding site, three truncated HTRA1 mutant plasmids were generated based on its known protein domain structure, and these constructs were

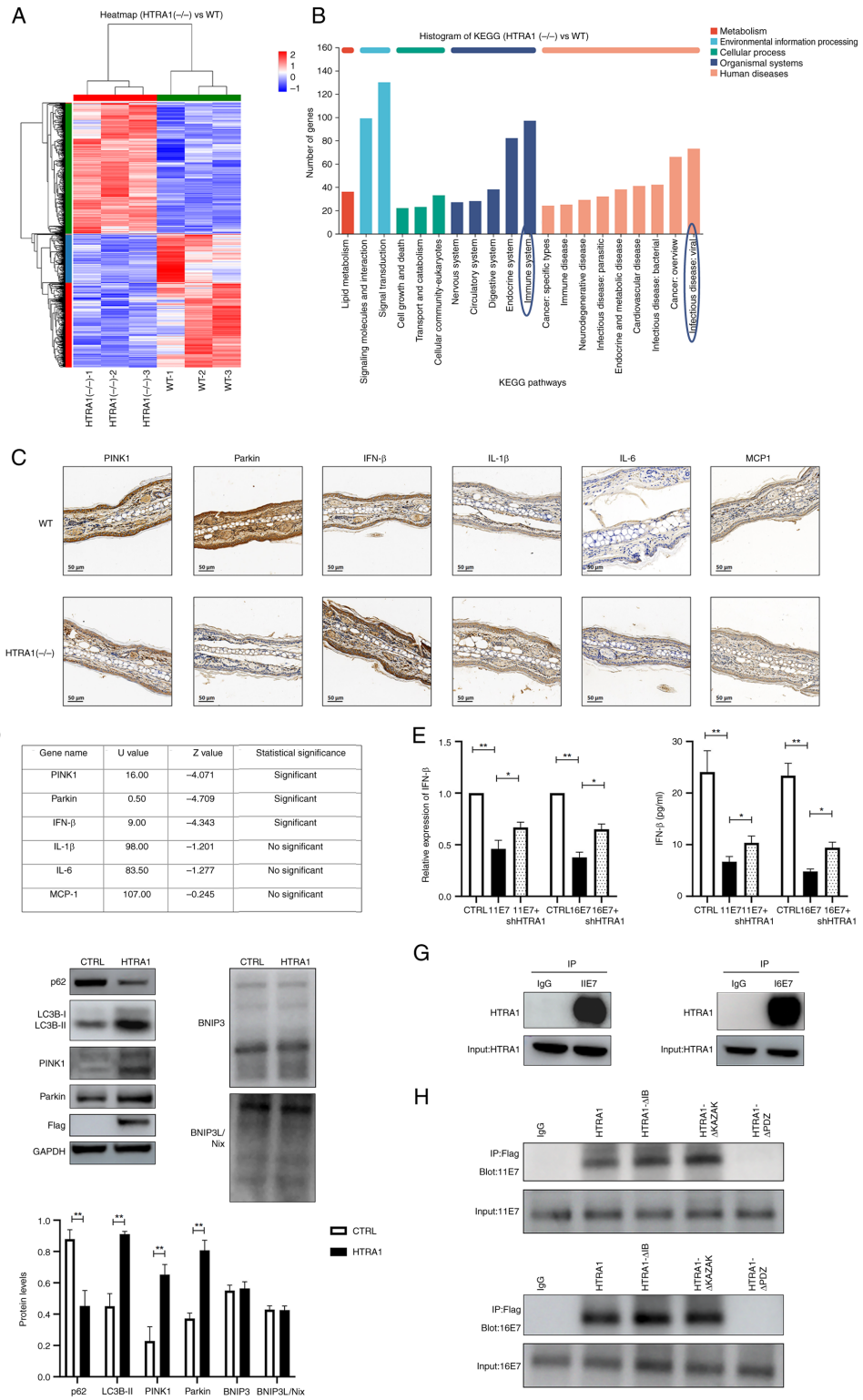

Figure 4. Knockout of HTRA1 can suppress mitophagy. (A) Heatmap illustrating the differential gene expression RNA-seq analysis of the skin of HTRA1(-/-) mice. For each sample, 1 μg total RNA was utilized to assess RNA integrity and construct libraries. A poly(A) mRNA selection system was employed to eliminate ribosomal RNA contamination. The purified RNA underwent reverse transcription, end-repairing, adapter ligation and PCR amplification prior to sequencing on the Illumina HiSeq 2500 platform. (B) KEGG pathway analysis of differentially expressed genes from the RNA-seq results of HTRA1(-/-) mouse skin. (C) Immunohistochemical assessment of PINK1, Parkin, IFN-β, IL-1β, IL-6 and MCP-1 expression in the ear tissues of WT and HTRA1(-/-) mice. (D) Mann-Whitney U test was employed to perform statistical analysis of the immunohistochemistry results. (E) Quantitative PCR and ELISA was employed to assess the levels of IFN-β in HPV11/16 E7-overexpressing NHEKs following HTRA1 gene knockdown. (F) Western blotting was performed to evaluate the expression levels of mitophagy-related markers and their associated signaling pathways in NHEK cells with HTRA1 overexpression (Flag tag). All protein expression levels were normalized to the loading control GAPDH. (G) IP was utilized to investigate the interaction between HPV E7 and HTRA1 in NHEKs. (H) Truncated HTRA1 plasmids were constructed and transfected into 293 cells overexpressing HPV E7. Next, IP was applied to identify the specific binding sites between HPV E7 and HTRA1. *P<0.05, **P<0.01. BNIP3, Bcl-2 and adenovirus E1B 19 kDa-interacting protein 3; BNIP3L, BNIP3-like; CTRL, control; HPV, human papillomavirus; HTRA1, high-temperature requirement A serine peptidase 1; IFN, interferon; IP, immunoprecipitation; KEGG, Kyoto Encyclopedia of Genes and Genomes; NHEK, normal human epidermal keratinocyte; PINK1, PTEN-induced kinase 1; RNA-seq, RNA sequencing; sh, short hairpin; WT, wild-type.

transfected into 293T cells stably overexpressing HPV E7 (Fig. S1C). Subsequent CO-IP analysis demonstrated that truncation of the PDZ domain in HTRA1 abolished the interaction between HPV E7 and HTRA1 (Fig. 4H). These findings confirm that HPV E7 specifically binds to the PDZ domain of HTRA1, suggesting that this domain is critical for molecular interaction.

Discussion

During the process of viral infection of epithelial cells, the early proteins of HPV exert a crucial role in the pathogenic process (6). The functions of the early proteins of HPV are both synergistic and notably distinct. Thus, exploring their individual functions holds great importance.

Previous studies have revealed that the HPV E7 protein can dampen the immune response of epithelial cells through multiple mechanisms, such as limiting the secretion of IFNs (83), suppressing the expression of pro-inflammatory cytokines, restraining the activity of antigen-presenting cells (65) and downregulating the activity of T cells (84,85), thus leading to persistent viral infection. Among these mechanisms, there are more studies on the inhibition of the secretion of type I IFNs. For example, HPV16/18 E7 affects the cGAS-STING pathway by interacting with NLRX1 and upregulating the expression of SUV39H1, thereby suppressing the production of type I IFNs. HPV18 E7 can also physically interact with interferon regulatory factor-1 (IRF1) and recruit histone deacetylases to the IFN-β promoter, thereby inhibiting the IRF1-mediated activation of the IFN-β promoter and blocking its transcription (87,88). Although previous studies have affirmed that HPV E7 can impact the immune response of epithelial cells, clinically, it is still not possible to eliminate persistent viral infections and patients continue to be affected by persistent HPV infection. Additionally, recent studies (89,90) have predominantly focused on high-risk HPV, while there are relatively fewer studies (91,92) on low-risk HPV. However, diseases related to low-risk HPV, such as condyloma acuminatum, have a high recurrence rate; therefore, it is of considerable importance to concurrently explore how high- and low-risk HPV E7 affect the local immune microenvironment. In the present study, both high- and low-risk HPV E7 were examined. Transmission electron microscopy, fluorescence co-localization and western blotting were applied to assess mitophagy levels in NHEKs overexpressing HPV11/16 E7, revealing that HPV E7 significantly enhanced mitophagy in these cells. The association between mitophagy and immune response requires further investigation.

In recent years, the role of energy metabolism in immune regulation has garnered increasing attention (93,94). Notably, certain organelles in eukaryotic cells have been implicated in the regulation of energy metabolism (23). Mitophagy, as a specific autophagic phenomenon for the selective elimination of damaged mitochondria, can impact the immune function of host cells through multiple pathways, including inhibiting the activation of inflammasomes (95,96), interfering with the expression of type I IFNs (97,98) and preventing the initiation of apoptosis in host cells (99,100), thereby affecting the cellular immune state. Numerous studies have focused on the influence of viruses on mitophagy in host cells. Viruses such as HBV, HCV, HSV and HIV can induce mitophagy in host cells to suppress innate immunity and sustain their persistent infection (101-103). However, at present, relatively few studies (48,104) have focused on the association between HPV and mitophagy. Several studies have investigated the relationship between HPV E7 and autophagy. For example, it has been confirmed that the expression of HPV16 E7 reduces the level of dual-specificity phosphatase 5, leading to activation of the MAPK/ERK signal, and the induction of classical autophagy through the mTOR and AMPK pathways (65). However, research investigating the association between HPV E7 and mitophagy remains limited. Notably, a previous study reported that high-risk HPV E7 could affect the mitophagy status of host cells (46); nevertheless, the specific mechanism remains unexplained, and to the best of our knowledge, no studies to date have focused on the association between low-risk HPV E7 and mitophagy. In the present study, two classical mitophagy pathways were assessed using western blotting. The results demonstrated that HPV E7 promoted mitophagy through the modulation of PINK1/Parkin and BNIP3/BNIP3L pathways Upon HTRA1 silencing, the expression of the PINK1/Parkin pathway was markedly reduced, whereas the BNIP3/BNIP3L pathway exhibited minimal downregulation, with no statistically significant changes observed. By contrast, HTRA1 overexpression alone significantly enhanced the activation of the PINK1/Parkin pathway. Collectively, these findings indicated that HPV E7 may regulate two distinct mitophagy pathways, while HTRA1 predominantly influences mitophagy via its effects on the PINK1/Parkin signaling axis.

HTRA1 is a non-glycosylated serine protease, which encompasses a C-terminal PDZ domain and an N-terminal insulin-like growth factor binding protein-like domain (105). Previous studies have demonstrated that HTRA1 is associated with various biological processes (106), regulates the occurrence and development of tumors (107), and interacts with TGF-β family proteins to regulate retinal angiogenesis as well as the survival and maturation of neurons during development (108). HTRA1 serves a role in diseases such as osteoarthritis (109,110), cartilage degeneration (111,112), coronary artery disease (113), cerebral small vessel disease (114) and macular degeneration (115). However, despite the identification of numerous functions at present, there are relatively limited studies (116,117) on the exploration in-depth of the function of HTRA1 protein. To date, to the best of our knowledge, no study has focused on the association between HPV and HTRA1, nor has the association between HTRA1 and mitophagy been explored. In the present study, Siha cells with stable knockdown of HPV16 E7 expression were employed for combined RNA-seq (transcriptional level) and iTRAQ (protein level) analyses. The results revealed that the expression of HTRA1 was decreased in the knockdown group. GO analysis suggested that HTRA1 was closely related to mitophagy. Furthermore, NHEKs overexpressing HPV11/16 E7 were utilized to verify that HPV E7 enhanced the expression of HTRA1 at the transcriptional and translational levels.

Additionally, HTRA1 knockdown in HPV11/16 E7-overexpressing NHEKs was achieved using shRNA. The results indicated that knockdown of HTRA1 significantly inhibited mitophagy in keratinocytes and restored the suppression of type I IFNs. Collectively, these findings suggested that

HPV E7 may enhance HTRA1 expression to activate the PINK1/Parkin pathway, thereby promoting mitophagy in host cells and influencing type I IFN expression, which ultimately affects the immune response of keratinocytes and facilitates persistent viral infection.

In the present study, IP was employed to ascertain whether HPV E7 and HTRA1 bind to each other to regulate their expression. The outcomes demonstrated that HPV E7 could directly bind to HTRA1 to impact its expression, which is in accordance with the literature (118). To further elucidate the direct interaction between HPV E7 and HTRA1, truncated mutant plasmids were constructed, and it was identified that HPV E7 specifically bound to the PDZ domain of HTRA1 to exert its biological function. In subsequent studies, we aim to further elucidate the exact binding motif of HPV E7 and the underlying molecular mechanisms by which this interaction upregulates HTRA1 expression, leading to modulation of the PINK1/Parkin signaling pathway and the regulation of mitophagy. Although HTRA1 is predominantly recognized as a secreted protein, accumulating evidence has demonstrated its functional role within intracellular compartments (61,119-121). The current study revealed that HTRA1 exhibited a detectable level of intracellular expression. Considering that HPV E7, as a viral oncoprotein, primarily executes its biological functions inside the cell, the present experimental data confirmed a direct interaction between HPV E7 and HTRA1. Based on these findings, it may be hypothesized that HPV E7 could modulate the expression and biological activities of HTRA1 through binding to its intracellularly localized form. The present findings suggested that HTRA1 serves a role in regulating the ubiquitin-dependent mitophagy pathway PINK1/Parkin, thereby promoting mitophagy. Further exploration is warranted regarding how HTRA1 affects this ubiquitin-related pathway. Furthermore, the current study revealed that HPV E7 could also influence the non-ubiquitinated mitophagy pathway BNIP3/BNIP3L; however, this effect did not occur through modulation of HTRA1. This mechanism is under further exploration. Our laboratory team is actively investigating the underlying molecular mechanisms to further elucidate the role of HTRA1 in the regulation of mitophagy. Future investigations should aim to elucidate the specific mechanisms by which HPV E7 impacts the BNIP3/BNIP3L pathway and further examine how HPV influences mitophagy.

At present, research on the relationship between HPV and mitophagy remains relatively limited. The current study has partially addressed this knowledge gap; however, several aspects of this research require further refinement. For example, the present study primarily focused on the regulatory role of the single HPV E7 gene in mitophagy, without examining the effects of complete HPV viral particles on host cell mitophagy. In future studies, we aim to simulate the natural infection process of HPV using pseudovirus infection models to further elucidate the underlying mechanisms by which the virus influences mitophagy, thereby enhancing the understanding of its association with persistent HPV infection.

Furthermore, additional investigation into the key gene HTRA1 is recommended to better understand its biological function and potential regulatory mechanisms. The present findings indicated that HTRA1 can independently induce mitophagy and that its expression is closely associated with this process. However, its impact on downstream immune signaling pathways remains unclear. In the next phase of our research, RNA-seq data from HTRA1(-/-) mice will be analyzed to identify and validate alterations in relevant immune-related genes and signaling pathways. This approach will allow for a systematic evaluation of the role of HTRA1 in immune regulation. Regarding clinical samples and translational applications, the preliminary observations of the current study suggested that HTRA1 expression may be elevated in tissues from patients positive for HPV11 and HPV16; however, the current sample size is limited. Our future study aims to expand the sample collection to include additional $HPV16^+$ cervical cancer tissues and $HPV11^+$ condyloma acuminatum specimens. All cervical cancer samples will be included in the analysis following pathological classification. Subsequently, we aim to employ immunohistochemical techniques to assess HTRA1 expression across samples and perform comparative analyses. Based on these results, stratified statistical and systematic analyses will be conducted to explore the potential associations between HTRA1 expression and clinical features. Ultimately, the aim for these findings is to provide a scientific foundation for the development of HTRA1-targeted therapeutics aimed at treating diseases associated with persistent HPV infection.

In conclusion, the present study indicated that HPV E7 could promote the expression of HTRA1 to activate the PINK1/Parkin pathway in keratinocytes, leading to enhanced mitophagy and reduced expression of type I IFN in host cells. The findings are expected to offer novel concepts and targets for the treatment of HPV persistent infection-related disorders.

Acknowledgements

Not applicable.

Funding

This study was supported by the National Natural Science Foundation of China (grant nos. 82103740 and 82471846) and the Science and Technology Projects of Zhejiang Province (grant no. 2022RC198).

Availability of data and materials

The data generated in the present study may be requested from the corresponding author. The RNA-seq data generated in the present study may be found in the Gene Expression Omnibus database under accession numbers GSE307971 and GSE308049, or at the following URLs:https://www.ncbi.nlm.nih.gov/geo/query/acc.cgi?acc=GSE307971 and https://www.ncbi.nlm.nih.gov/geo/query/acc.cgi?acc=GSE308049, respectively.

Authors' contributions

HC and XS confirm the authenticity of all the raw data. HC, XS and BZ designed the research. XS, BZ, SC and DK performed the research. BZ, SC and DK analyzed the data and all authors interpreted the data. BZ drafted the manuscript. HC and XS revised the manuscript content. HC takes responsibility for the

integrity of the data. All authors read and approved the final manuscript.

Ethics approval and consent to participate

All experimental procedures involving mice were approved by the Medical Ethics Committee of Sir Run Run Shaw Hospital, Zhejiang University School of Medicine (approval no. 202402156; Hangzhou, China). All human samples were collected following the collection of written informed consent from the research participants. All experimental procedures involving human tissues were approved by the Medical Ethics Committee of Sir Run Run Shaw Hospital, Zhejiang University School of Medicine (approval nos. 20210923-39 and 2021072 9-263). The NHEKs used in the present study purchased from ScienCell Research Laboratories, Inc. The Medical Ethics Committee of Sir Run Run Shaw Hospital, Zhejiang University School of Medicine has confirmed that ethics approval is not required for the use of these cells.

Patient consent for publication

Written informed consent was obtained from all patients prior to their participation in the current study, including consent for publication of the present study.

Competing interests

The authors declare that they have no competing interests.

References

1. Doorbar J, Quint W, Banks L, Bravo IG, Stoler M, Broker TR and Stanley MA: The biology and life-cycle of human papillomaviruses. Vaccine 30 Suppl 5: F55-F70, 2012.
2. Woodworth CD: HPV innate immunity. Front Biosci 7: d2058-d2071, 2002.
3. Chen L, Hu H, Pan Y, Lu Y, Zhao M, Zhao Y, Wang L, Liu K and Yu Z: The role of HPV11 E7 in modulating STING-dependent interferon β response in recurrent respiratory papillomatosis. J Virol 98: e0192523, 2024.
4. Doorbar J, Egawa N, Griffin H, Kranjec C and Murakami I: Human papillomavirus molecular biology and disease association. Rev Med Virol 25 (Suppl 1): S2-S23, 2015.
5. Crosbie EJ, Einstein MH, Franceschi S and Kitchener HC: Human papillomavirus and cervical cancer. Lancet 382: 889-899, 2013.
6. McBride AA: Oncogenic human papillomaviruses. Philos Trans R Soc Lond B Biol Sci 372: 20160273, 2017.
7. Duensing S and Münger K: The human papillomavirus type 16 E6 and E7 oncoproteins independently induce numerical and structural chromosome instability. Cancer Res 62: 7075-7082, 2002.
8. Klingelhutz AJ and Roman A: Cellular transformation by human papillomaviruses: lessons learned by comparing high- and low-risk viruses. Virology 424: 77-98, 2012.
9. Zhang B, Chen W and Roman A: The E7 proteins of low- and high-risk human papillomaviruses share the ability to target the pRB family member p130 for degradation. Proc Natl Acad Sci USA 103: 437-442, 2006.
10. Münger K, Werness BA, Dyson N, Phelps WC, Harlow E and Howley PM: Complex formation of human papillomavirus E7 proteins with the retinoblastoma tumor suppressor gene product. EMBO J 8: 4099-4105, 1989.
11. Dyson N, Howley PM, Münger K and Harlow E: The human papilloma virus-16 E7 oncoprotein is able to bind to the retinoblastoma gene product. Science 243: 934-937, 1989.
12. Boulet G, Horvath C, Vanden Broeck D, Sahebali S and Bogers J: Human papillomavirus: E6 and E7 oncogenes. Int J Biochem Cell Biol 39: 2006-2011, 2007.
13. Ryser MD, Rositch A and Gravitt PE: Modeling of US human papillomavirus (HPV) seroprevalence by age and sexual behavior indicates an increasing trend of HPV infection following the sexual revolution. J Infect Dis 216: 604-611, 2017.
14. Forman D, de Martel C, Lacey CJ, Soerjomataram I, Lortet-Tieulent J, Bruni L, Vignat J, Ferlay J, Bray F, Plummer M and Franceschi S: Global Burden of Human Papillomavirus and Related Diseases. Vaccine 30 (Suppl 5): F12-F23, 2012.
15. Yang X, Li Y, Tang Y, Li Z, Wang S, Luo X, He T, Yin A and Luo M: Cervical HPV infection in Guangzhou, China: An epidemiological study of 198,111 women from 2015 to 2021. Emerg Microbes Infect 12: e2176009, 2023.
16. Han S, Lin M, Liu M, Wu S, Guo P, Guo J, Xie L, Qiu S, Xu A, Cai Y and Chen Y: Prevalence, trends, and geographic distribution of human papillomavirus infection in Chinese women: A summative analysis of 2,728,321 cases. BMC Med 23: 158, 2025.
17. Crow JM: HPV: The global burden. Nature 488: S2-S3, 2012.
18. Wang J, Elfström KM and Dillner J: Human papillomavirus-based cervical screening and long-term cervical cancer risk: A randomised health-care policy trial in Sweden. Lancet Public Health 9: e886-e895, 2024.
19. Graham SV: The human papillomavirus replication cycle, and its links to cancer progression: A comprehensive review. Clin Sci (Lond) 131: 2201-2221, 2017.
20. zur Hausen H: Papillomaviruses in the causation of human cancers-a brief historical account. Virology 384: 260-265, 2009.
21. del Pino M, Bleeker MC, Quint WG, Snijders PJ, Meijer CJ and Steenbergen RD: Comprehensive analysis of human papillomavirus prevalence and the potential role of low-risk types in verrucous carcinoma. Mod Pathol 25: 1354-1363, 2012.
22. Jamshidi M, Shekari M, Nejatizadeh A, Malekzadeh K, Baghershiroodi M, Davudian P, Dehghan F and Jamshidi F: The impact of human papillomavirus (HPV) types 6, 11 in women with genital warts. Arch Gynecol Obstet 286: 1261-1267, 2012.
23. Friedman JR and Nunnari J: Mitochondrial form and function. Nature 505: 335-343, 2014.
24. Gkikas I, Palikaras K and Tavernarakis N: The role of mitophagy in innate immunity. Front Immunol 9: 1283, 2018.
25. Mehta MM, Weinberg SE and Chandel NS: Mitochondrial control of immunity: Beyond ATP. Nat Rev Immunol 17: 608-620, 2017.
26. Mills EL, Kelly B and O'Neill LAJ: Mitochondria are the powerhouses of immunity. Nat Immunol 18: 488-498, 2017.
27. Onishi M, Yamano K, Sato M, Matsuda N and Okamoto K: Molecular mechanisms and physiological functions of mitophagy. EMBO J 40: e104705, 2021.
28. Zhang L, Qin Y and Chen M: Viral strategies for triggering and manipulating mitophagy. Autophagy 14: 1665-1673, 2018.
29. Moehlman AT and Youle RJ: Mitochondrial quality control and restraining innate immunity. Annu Rev Cell Dev Biol 36: 265-289, 2020.
30. Kim MJ, Bae SH, Ryu JC, Kwon Y, Oh JH, Kwon J, Moon JS, Kim K, Miyawaki A, Lee MG, *et al*: SESN2/sestrin2 suppresses sepsis by inducing mitophagy and inhibiting NLRP3 activation in macrophages. Autophagy 12: 1272-1291, 2016.
31. Qi N, Shi Y, Zhang R, Zhu W, Yuan B, Li X, Wang C, Zhang X and Hou F: Multiple truncated isoforms of MAVS prevent its spontaneous aggregation in antiviral innate immune signalling. Nat Commun 8: 15676, 2017.
32. Jena KK, Mehto S, Nath P, Chauhan NR, Sahu R, Dhar K, Das SK, Kolapalli SP, Murmu KC, Jain A, *et al*: Autoimmunity gene IRGM suppresses cGAS-STING and RIG-I-MAVS signaling to control interferon response. EMBO Rep 21: e50051, 2020.
33. Bu L, Wang H, Hou P, Guo S, He M, Xiao J, Li P, Zhong Y, Jia P, Cao Y, *et al*: The Ubiquitin E3 ligase parkin inhibits innate antiviral immunity through K48-linked polyubiquitination of RIG-I and MDA5. Front Immunol 11: 1926, 2020.
34. Sliter DA, Martinez J, Hao L, Chen X, Sun N, Fischer TD, Burman JL, Li Y, Zhang Z, Narendra DP, *et al*: Parkin and PINK1 mitigate STING-induced inflammation. Nature 561: 258-262, 2018.
35. Kim SJ, Khan M, Quan J, Till A, Subramani S and Siddiqui A: Hepatitis B virus disrupts mitochondrial dynamics: Induces fission and mitophagy to attenuate apoptosis. PLoS Pathog 9: e1003722, 2013.
36. Adriaenssens E, Nguyen TN, Sawa-Makarska J, Khuu G, Schuschnig M, Shoebridge S, Skulsuppaisarn M, Watts EM, Csalyi KD, Padman BS, *et al*: Control of mitophagy initiation and progression by the TBK1 adaptors NAP1 and SINTBAD. Nat Struct Mol Biol 31: 1717-1731, 2024.

37. Zhao X, Wang Z, Wang L, Jiang T, Dong D and Sun M: The PINK1/Parkin signaling pathway-mediated mitophagy: A forgotten protagonist in myocardial ischemia/reperfusion injury. Pharmacol Res 209: 107466, 2024.
38. O'Sullivan TE, Johnson LR, Kang HH and Sun JC: BNIP3- and BNIP3L-mediated mitophagy promotes the generation of natural killer cell memory. Immunity 43: 331-342, 2015.
39. Zhang B, Xu S, Liu M, Wei Y, Wang Q, Shen W, Lei CQ and Zhu Q: The nucleoprotein of influenza A virus inhibits the innate immune response by inducing mitophagy. Autophagy 19: 1916-1933, 2023.
40. Sun Z, Ma Z, Cao W, Jiang C, Guo L, Liu K, Gao Y, Bai J, Pi J, Jiang P and Liu X: Calcium-mediated mitochondrial fission and mitophagy drive glycolysis to facilitate arterivirus proliferation. PLoS Pathog 21: e1012872, 2025.
41. Khan M, Syed GH, Kim SJ and Siddiqui A: Hepatitis B virus-induced parkin-dependent recruitment of linear ubiquitin assembly complex (LUBAC) to mitochondria and attenuation of innate immunity. PLoS Pathog 12: e1005693, 2016.
42. Vo MT, Smith BJ, Nicholas J and Choi YB: Activation of NIX-mediated mitophagy by an interferon regulatory factor homologue of human herpesvirus. Nat Commun 10: 3203, 2019.
43. Kim SJ, Syed GH and Siddiqui A: Hepatitis C virus induces the mitochondrial translocation of Parkin and subsequent mitophagy. PLoS Pathog 9: e1003285, 2013.
44. Ojeda DS, Grasso D, Urquiza J, Till A, Vaccaro MI and Quarleri J: Cell death is counteracted by mitophagy in HIV-productively infected astrocytes but is promoted by inflammasome activation among non-productively infected cells. Front Immunol 9: 2633, 2018.
45. Perkins DN, Pappin DJ, Creasy DM and Cottrell JS: Probability-based protein identification by searching sequence databases using mass spectrometry data. Electrophoresis 20: 3551-3567, 1999.
46. Thomas RJ, Oleinik N, Panneer Selvam S, Vaena SG, Dany M, Nganga RN, Depalma R, Baron KD, Kim J, Szulc ZM and Ogretmen B: HPV/E7 induces chemotherapy-mediated tumor suppression by ceramide-dependent mitophagy. EMBO Mol Med 9: 1030-1051, 2017.
47. Russell WMS and Burch RL: The Principles of Humane Experimental Technique. Methuen & Co., Ltd., London, 1959.
48. American Veterinary Medical Association (AVMA): AVMA Guidelines for the euthanasia of animals: 2013 Edition. AVMA, Schaumburg, IL 2013.
49. Chen S, Zhou Y, Chen Y and Gu J: fastp: An ultra-fast all-in-one FASTQ preprocessor. Bioinformatics 34: i884-i890, 2018.
50. Kim D, Langmead B and Salzberg SL: HISAT: A fast spliced aligner with low memory requirements. Nat Methods 12: 357-360, 2015.
51. Pertea M, Pertea GM, Antonescu CM, Chang TC, Mendell JT and Salzberg SL: StringTie enables improved reconstruction of a transcriptome from RNA-seq reads. Nat Biotechnol 33: 290-295, 2015.
52. Love MI, Huber W and Anders S: Moderated estimation of fold change and dispersion for RNA-seq data with DESeq2. Genome Biol 15: 550, 2014.
53. Wang L, Feng Z, Wang X, Wang X and Zhang X: DEGseq: An R package for identifying differentially expressed genes from RNA-seq data. Bioinformatics 26: 136-138, 2010.
54. Klopfenstein DV, Liangsheng Z, Pedersen BS, Ramírez F, Warwick Vesztrocy A, Naldi A, Mungall CJ, Yunes JM, Botvinnik O, Weigel M, *et al*: GOATOOLS: A python library for Gene ontology analyses. Sci Rep 8: 10872, 2018.
55. Kanehisa M, Furumichi M, Sato Y, Matsuura Y and Ishiguro-Watanabe M: KEGG: Biological systems database as a model of the real world. Nucleic Acids Res 53(D1): D672-D677, 2025.
56. Langfelder P and Horvath S: WGCNA: An R package for weighted correlation network analysis. BMC Bioinformatics 9: 559, 2008.
57. Shen S, Park JW, Lu ZX, Lin L, Henry MD, Wu YN, Zhou Q and Xing Y: rMATS: Robust and flexible detection of differential alternative splicing from replicate RNA-Seq data. Proc Natl Acad Sci USA 111: E5593-E5601, 2014.
58. Jiang X, Arrey T, Damoc E, Scigelova M, Horn D, Viner R and Huhmer AFR: TMT Workflow on the Q Exactive Series-Instrument Parameter Optimization and Data Analysis in Proteome Discoverer 2.1 Software. Thermo Fisher Scientific Inc., 2016.
59. Apweiler R, Bairoch A, Wu CH, Barker WC, Boeckmann B, Ferro S, Gasteiger E, Huang H, Lopez R, Magrane M, *et al*: UniProt: The universal protein knowledgebase. Nucleic Acids Res 32(Database issue): D115-D119, 2004.
60. De Luca A, De Falco M, Severino A, Campioni M, Santini D, Baldi F, Paggi MG and Baldi A: Distribution of the serine protease HtrA1 in normal human tissues. J Histochem Cytochem 51: 1279-1284, 2003.
61. Shi H, Yuan M, Cai J, Lan L, Wang Y, Wang W, Zhou J, Wang B, Yu W, Dong Z, *et al*: HTRA1-driven detachment of type I collagen from endoplasmic reticulum contributes to myocardial fibrosis in dilated cardiomyopathy. J Transl Med 22: 297, 2024.
62. Ding Y, Jiang S, Chen X, Chen L, Zhang X and Cheng H: Expression and polyclonal antibody preparation of HPV-11E7 protein. Xi Bao Yu Fen Zi Mian Yi Xue Za Zhi 30: 618-622, 2014 (In Chinese).
63. Cao L, Cheng H, Wang H, Zhou Q, Tang Z, Jiang S, Ding Y and Chen X: Research on the Detection of *Condyloma Acuminatum* Lesions Using Self-prepared Polyclonal Antibodies against HPV6b and 11 E7 Proteins. Chin J Dermatol 11: 774-777, 2015 (In Chinese).
64. Hua C, Zheng Q, Zhu J, Chen S, Song Y, van der Veen S and Cheng H: Human papillomavirus type 16 early protein E7 activates autophagy through inhibition of dual-specificity phosphatase 5. Oxid Med Cell Longev 2022: 1863098, 2022.
65. Song Y, Wu X, Xu Y, Zhu J, Li J, Zou Z, Chen L, Zhang B, Hua C, Rui H, *et al*: HPV E7 inhibits cell pyroptosis by promoting TRIM21-mediated degradation and ubiquitination of the IFI16 inflammasome. Int J Biol Sci 16: 2924-2937, 2020.
66. Livak KJ and Schmittgen TD: Analysis of relative gene expression data using real-time quantitative PCR and the 2(-Delta Delta C(T)) Method. Methods 25: 402-408, 2001.
67. Qin X, Chen H, Zhu X, Xu X and Gao J: Identification of Rab7 as an autophagy marker: Potential therapeutic approaches and the effect of Qi Teng Xiao Zhuo granule in chronic glomerulonephritis. Pharm Biol 61: 1120-1134, 2023.
68. Klionsky DJ, Abdel-Aziz AK, Abdelfatah S, Abdellatif M, Abdoli A, Abel S, Abeliovich H, Abildgaard MH, Abudu YP, Acevedo-Arozena A *et al*: Guidelines for the use and interpretation of assays for monitoring autophagy (4th edition). Autophagy 17: 1-382, 2021.
69. Barbaro V, Testa A, Di Iorio E, Mavilio F, Pellegrini G and De Luca M: C/EBPδ regulates cell cycle and self-renewal of human limbal stem cells. J Cell Biol 177: 1037-1049, 2007.
70. Rahman MS, Kang I, Lee Y, Habib MA, Choi BJ, Kang JS, Park DS and Kim YS: Bifidobacterium longum subsp. infantis YB0411 inhibits adipogenesis in 3T3-L1 pre-adipocytes and reduces high-fat-diet-induced obesity in mice. J Agric Food Chem 69: 6032-6042, 2021.
71. Malpartida AB, Williamson M, Narendra DP, Wade-Martins R and Ryan BJ: Mitochondrial dysfunction and mitophagy in Parkinson's disease: From mechanism to therapy. Trends Biochem Sci 46: 329-343, 2021.
72. Song SN, Li HJ, Liang JL, Ren QQ, Li CX and Xu SY: Lentivirus-mediated missense mutation in HtrA1 leads to activation of the TGF-β/Smads pathway and increased apoptosis of mouse brain microvascular endothelial cells via the oxidative stress pathway. J Integr Neurosci 23: 201, 2024.
73. Lee J, Huh S, Park K, Kang N, Yu HS, Park HG, Kim YS, Kang UG, Won S and Kim SH: Behavioral and transcriptional effects of repeated electroconvulsive seizures in the neonatal MK-801-treated rat model of schizophrenia. Psychopharmacology (Berl) 241: 817-832, 2023.
74. Barnard SJ, Haunschild J, Heiser L, Dieterlen MT, Klaeske K, Borger MA and Etz CD: Apoptotic cell death in bicuspid-aortic-valve-associated aortopathy. Int J Mol Sci 24: 7429, 2023.
75. Gutiérrez-Muñoz C, Blázquez-Serra R, San Sebastian-Jaraba I, Sanz-Andrea S, Fernández-Gómez MJ, Nuñez-Moreno G, Mínguez P, Escolá-Gil JC, Nogales P, Ollivier V, *et al*: Annexin A8 deficiency delays atherosclerosis progression. Clin Transl Med 15: e70176, 2025.
76. Zhou GZ, Sun YH, Shi YY, Zhang Q, Zhang L, Cui LQ and Sun GC: ANXA8 regulates proliferation of human non-small lung cancer cells A549 via EGFR-AKT-mTOR signaling pathway. Mol Biol (Mosk) 55: 870-880, 2021.
77. Wei Y, Li Q, He K, Liao G, Cheng L, Li M and He Z: Mechanism of cigarette smoke in promoting small airway remodeling in mice via STAT 3 / PINK 1-Parkin / EMT. Free Radic Biol Med 224: 447-456, 2024.

78. Yan J, Chen X, Choksi S and Liu ZG: TGFB signaling induces mitophagy via PLSCR3-mediated cardiolipin externalization in conjunction with a BNIP3L/NIX-, BNIP3-, and FUNDC1-dependent mechanism. Autophagy 21: 1791-1801, 2025.
79. Adriaenssens E, Schaar S, Cook ASI, Stuke JFM, Sawa-Makarska J, Nguyen TN, Ren X, Schuschnig M, Romanov J, Khuu G, *et al*: Reconstitution of BNIP3/NIX-mitophagy initiation reveals hierarchical flexibility of the autophagy machinery. Nat Cell Biol 27: 1272-1287, 2025.
80. Yan T, Li H, Yan J, Ma S and Tan J: Age-related mitophagy regulates orthodontic tooth movement by affecting PDLSCs mitochondrial function and RANKL/OPG. FASEB J 38: e23865, 2024.
81. Stuqui B, Conceição AL, Termini L, Sichero L, Villa LL, Rahal P and Calmon MF: The differential role of HTRA1 in HPV-positive and HPV-negative cervical cell line proliferation. BMC Cancer 16: 840, 2016.
82. Chien J, Ota T, Aletti G, Shridhar R, Boccellino M, Quagliuolo L, Baldi A and Shridhar V: Serine protease HtrA1 associates with microtubules and inhibits cell migration. Mol Cell Biol 29: 4177-4187, 2009.
83. Antonsson A, Payne E, Hengst K and McMillan N: The human papillomavirus type 16 E7 protein binds human interferon regulatory factor-9 via a novel PEST domain required for transformation. J Interferon Cytokine Res 26: 455-461, 2006.
84. Martínez-Campos C, Burguete-García AI and Madrid-Marina V: Role of TLR9 in oncogenic virus-produced cancer. Viral Immunol 30: 98-105, 2017.
85. Pacini L, Savini C, Ghittoni R, Saidj D, Lamartine J, Hasan UA, Accardi R and Tommasino M: Downregulation of toll-like receptor 9 expression by beta human papillomavirus 38 and implications for cell cycle control. J Virol 89: 11396-11405, 2015.
86. Lo Cigno I, Calati F, Borgogna C, Zevini A, Albertini S, Martuscelli L, De Andrea M, Hiscott J, Landolfo S and Gariglio M: Human papillomavirus E7 oncoprotein subverts host innate immunity via SUV39H1-mediated epigenetic silencing of immune sensor genes. J Virol 94: e01812-19, 2020.
87. Park JS, Kim EK, Kwon HJ, Hwang ES, Namkoong SE and Um SJ: Inactivation of interferon regulatory factor-1 tumor suppressor protein by HPV E7 oncoprotein. Implication for the E7-mediated immune evasion mechanism in cervical carcinogenesis. J Biol Chem 275: 6764-6769, 2000.
88. Um SJ, Rhyu JW, Kim EJ, Jeon KC, Hwang ES and Park JS: Abrogation of IRF-1 response by high-risk HPV E7 protein in vivo. Cancer Lett 179: 205-212, 2002.
89. 91. Ray J, Baidya J, Paul DP, Majumdar G, Debbarma S, Sarkar A, Chakma M, Barman MP, Pattnaik M, Debnath A and Nath S: Molecular epidemiology and genotype distribution of genital high-risk human papillomavirus among women in North-East India. Egypt J Med Hum Genet 26: 114, 2025.
90. Hongo T, Yamamoto H, Tanabe M, Yasumatsu R, Kuga R, Miyazaki Y, Jiromaru R, Hashimoto K, Tateishi Y, Sonoda KH, *et al*: High-risk HPV-related squamous cell carcinoma in the conjunctiva and lacrimal sac: Clinicopathologic characteristics and diagnostic utility of p16 and Rb immunohistochemistry. Am J Surg Pathol 46: 977-987, 2022.
91. Wolf J, Kist LF, Pereira SB, Quessada MA, Petek H, Pille A, Maccari JG, Mutlaq MP and Nasi LA: Human papillomavirus infection: Epidemiology, biology, host interactions, cancer development, prevention, and therapeutics. Rev Med Virol 34: e2537, 2024.
92. Shah KD, Chamseddine I, Yuan X, Tian S, Qiu R, Zhou J, Dhabaan A, Al-Hallaq H, Yu DS, Paganetti H and Yang X: Clinically interpretable survival risk stratification in head and neck cancer using bayesian networks and markov blankets. Int J Radiat Oncol Biol Phys: S0360-3016 (25) 06336-9, Oct 11, 2025 (Epubahead of print).
93. Niu Y, Nie Q, Dong L, Zhang J, Liu SF, Song W, Wang X, Wu G and Song D: Hydrogen attenuates allergic inflammation by reversing energy metabolic pathway switch. Sci Rep 10: 1962, 2020.
94. Savagner F, Farge T, Karim Z and Aloulou M: Iron and energy metabolic interactions in Treg-mediated immune regulation. Front Immunol 16: 1554028, 2025.
95. Gupta S, Cassel SL, Sutterwala FS and Dagvadorj J: Regulation of the NLRP3 inflammasome by autophagy and mitophagy. Immunol Rev 329: e13410, 2025.
96. Tao G, Wang X, Wang J, Ye Y, Zhang M, Lang Y and Ding S: Dihydro-resveratrol ameliorates NLRP3 inflammasome-mediated neuroinflammation via Bnip3-dependent mitophagy in Alzheimer's disease. Br J Pharmacol 182: 1005-1024, 2025.
97. Zhao Y, Ding C, Zhu Z, Wang W, Wen W, Favoreel HW and Li X: Pseudorabies virus infection triggers mitophagy to dampen the interferon response and promote viral replication. J Virol 98: e0104824, 2024.
98. Cheng J, Wang Y, Yin L, Liang W, Zhang J, Ma C, Zhang Y, Liu B, Wang J, Zhao W, *et al*: The nonstructural protein 1 of respiratory syncytial virus hijacks host mitophagy as a novel mitophagy receptor to evade the type I IFN response in HEp-2 cells. mBio 14: e0148023, 2023.
99. Weng W, He Z, Ma Z, Huang J, Han Y, Feng Q, Qi W, Peng Y, Wang J, Gu J, *et al*: Tufm lactylation regulates neuronal apoptosis by modulating mitophagy in traumatic brain injury. Cell Death Differ 32: 530-545, 2025.
100. Gu B, Yu W, Huang Z, Bai J, Liu S, Ren B, Wang P, Sun L, Wen J, Zheng Y, *et al*: MRG15 promotes cell apoptosis through inhibition of mitophagy in hyperlipidemic acute pancreatitis. Apoptosis 30: 149-166, 2025.
101. Lee J and Ou JJ: HCV-induced autophagy and innate immunity. Front Immunol 15: 1305157, 2024.
102. Song X, Wang Y, Zou W, Wang Z, Cao W, Liang M, Li F, Zeng Q, Ren Z, Wang Y and Zheng K: Inhibition of mitophagy via the EIF2S1-ATF4-PRKN pathway contributes to viral encephalitis. J Adv Res 73: 199-217, 2025.
103. Figarola-Centurión I, Escoto-Delgadillo M, González-Enríquez GV, Gutiérrez-Sevilla JE, Vázquez-Valls E, Cárdenas-Bedoya J and Torres-Mendoza BM: HIV-1 Tat induces dysregulation of PGC1-Alpha and Sirtuin 3 expression in neurons: The role of mitochondrial biogenesis in HIV-Associated neurocognitive disorder (HAND). Int J Mol Sci 24: 17566, 2023.
104. Toyohara Y, Taguchi A, Ishii Y, Yoshimoto D, Yamazaki M, Matsunaga H, Nakatani K, Hoshi D, Tsuchimochi S, Kusakabe M, *et al*: Identification of target cells of human papillomavirus 18 using squamocolumnar junction organoids. Cancer Sci 115: 125-138, 2024.
105. Chien J, Aletti G, Baldi A, Catalano V, Muretto P, Keeney GL, Kalli KR, Staub J, Ehrmann M, Cliby WA, *et al*: Serine protease HtrA1 modulates chemotherapy-induced cytotoxicity. J Clin Invest 116: 1994-2004, 2006.
106. Clausen T, Southan C and Ehrmann M: The HtrA family of proteases: Implications for protein composition and cell fate. Mol Cell 10: 443-455, 2002.
107. Klose R, Adam MG, Weis EM, Moll I, Wüstehube-Lausch J, Tetzlaff F, Oka C, Ehrmann M and Fischer A: Inactivation of the serine protease HTRA1 inhibits tumor growth by deregulating angiogenesis. Oncogene 37: 4260-4272, 2018.
108. Beaufort N, Scharrer E, Kremmer E, Lux V, Ehrmann M, Huber R, Houlden H, Werring D, Haffner C and Dichgans M: Cerebral small vessel disease-related protease HtrA1 processes latent TGF-β binding protein 1 and facilitates TGF-β signaling. Proc Natl Acad Sci USA 111: 16496-501, 2014.
109. Grau S, Richards PJ, Kerr B, Hughes C, Caterson B, Williams AS, Junker U, Jones SA, Clausen T and Ehrmann M: The role of human HtrA1 in arthritic disease. J Biol Chem 281: 6124-6129, 2006.
110. Bhutada S, Hoyle A, Piuzzi NS and Apte SS: Degradomics defines proteolysis information flow from human knee osteoarthritis cartilage to matched synovial fluid and the contributions of secreted proteases ADAMTS5, MMP13 and CMA1 to articular cartilage breakdown. Osteoarthritis Cartilage 33: 116-127, 2025.
111. Tossetta G, Fantone S, Licini C, Marzioni D and Mattioli-Belmonte M: The multifaced role of HtrA1 in the development of joint and skeletal disorders. Bone 157: 116350, 2022.
112. Tiaden AN, Klawitter M, Lux V, Mirsaidi A, Bahrenberg G, Glanz S, Quero L, Liebscher T, Wuertz K, Ehrmann M and Richards PJ: Detrimental role for human high temperature requirement serine protease A1 (HTRA1) in the pathogenesis of intervertebral disc (IVD) degeneration. J Biol Chem 287: 21335-21345, 2012.
113. Malik R, Beaufort N, Li J, Tanaka K, Georgakis MK, He Y, Koido M, Terao C, Japan B, Anderson CD, *et al*: Genetically proxied HTRA1 protease activity and circulating levels independently predict risk of ischemic stroke and coronary artery disease. Nat Cardiovasc Res 3: 701-713, 2024.
114. Li Y, Ying Y, Yao T, Jia X, Liang H, Tang W, Jia X, Song H, Shao X, Wang DJJ, *et al*: Decreased water exchange rate across blood-brain barrier in hereditary cerebral small vessel disease. Brain 146: 3079-3087, 2023.

115. Beguier F, Housset M, Roubeix C, Augustin S, Zagar Y, Nous C, Mathis T, Eandi C, Benchaboune M, Drame-Maigné A, *et al*: The 10q26 risk haplotype of age-related macular degeneration aggravates subretinal inflammation by impairing monocyte elimination. Immunity 53, 2020.
116. Jiang Z, Li X, Liu F, Li J, Yang K, Xu S and Jiang Z: Downregulation of HTRA1 Promotes EMT and anoikis resistance in colorectal cancer via activation of Hippo/YAP1 pathway by facilitating LATS2 degradation. Mol Carcinog 64: 1330-1346, 2025.
117. Eigenbrot C, Ultsch M, Lipari MT, Moran P, Lin SJ, Ganesan R, Quan C, Tom J, Sandoval W, van Lookeren Campagne M and Kirchhofer D: Structural and functional analysis of HtrA1 and its subdomains. Structure 20: 1040-1050, 2012.
118. Clawson GA, Bui V, Xin P, Wang N and Pan W: Intracellular localization of the tumor suppressor HtrA1/Prss11 and its association with HPV16 E6 and E7 proteins. J Cell Biochem 105: 81-88, 2008.
119. Xu W, Liu X, Han W, Wu K, Zhao M, Mei T, Shang B, Wu J, Luo J, Lai Y, *et al*: Inhibiting HIF-1 signaling alleviates HTRA1-induced RPE senescence in retinal degeneration. Cell Commun Signal 21: 134, 2023.
120. Guo F, Tao X, Wu Y, Dong D, Zhu Y, Shang D and Xiang H: Carfilzomib relieves pancreatitis-initiated pancreatic ductal adenocarcinoma by inhibiting high-temperature requirement protein A1. Cell Death Discov 10: 58, 2024.
121. Liu W, Liu C, Xiao J, Qian C, Chen Z, Lin W, Zhang Y, Wu J, Zhou R and Zhao L: HTRA1 interacts with SLC7A11 to modulate colorectal cancer chemosensitivity by inhibiting ferroptosis. Cell Death Discov 10: 228, 2024.